Frontiers of Information Technology & Electronic Engineering
www.jzus.zju.edu.cn; engineering.cae.cn; www.springerlink.com
ISSN 2095-9184 (print); ISSN 2095-9230 (online)
E-mail: jzus@zju.edu.cn

On optimization of cooperative MIMO for underlaid secrecy Industrial Internet of Things*

Xinyao WANG[1], Xuyan BAO[2], Yuzhen HUANG[3], Zhong ZHENG[†‡1], Zesong FEI[1]

[1]*School of Information and Electronics, Beijing Institute of Technology, Beijing 100081, China*

[2]*China Academy of Information and Communications Technology, Beijing 100191, China*

[3]*Academy of Military Sciences of PLA, Beijing 100091, China*

[†]E-mail: zhong.zheng@bit.edu.cn

Received May 5, 2022; Revision accepted Oct. 10, 2022; Crosschecked Feb. 3, 2023

Abstract: In this paper, physical layer security techniques are investigated for cooperative multi-input multi-output (C-MIMO), which operates as an underlaid cognitive radio system that coexists with a primary user (PU). The underlaid secrecy paradigm is enabled by improving the secrecy rate towards the C-MIMO receiver and reducing the interference towards the PU. Such a communication model is especially suitable for implementing Industrial Internet of Things (IIoT) systems in the unlicensed spectrum, which can trade off spectral efficiency and information secrecy. To this end, we propose an eigenspace-adaptive precoding (EAP) method and formulate the secrecy rate optimization problem, which is subject to both the single device power constraint and the interference power constraint. This precoder design is enabled by decomposing the original optimization problem into eigenspace selection and power allocation sub-problems. Herein, the eigenvectors are adaptively selected by the transmitter according to the channel conditions of the underlaid users and the PUs. In addition, a simplified EAP method is proposed for large-dimensional C-MIMO transmission, exploiting the additional spatial degree of freedom for a low-complexity secrecy precoder design. Numerical results show that by transmitting signal and artificial noise in the properly selected eigenspace, C-MIMO can eliminate the secrecy outage and outperforms the fixed eigenspace precoding methods. Moreover, the proposed simplified EAP method for the large-dimensional C-MIMO can significantly improve the secrecy rate.

Key words: Cognitive radio network; Physical layer security; Cooperative multi-input multi-output (C-MIMO); Eigenspace-adaptive precoding; Difference convex programming

https://doi.org/10.1631/FITEE.2200188 **CLC number:** TN92

1 Introduction

1.1 Background

The Industrial Internet of Things (IIoT) is one of the most important applications of beyond 5$^{\text{th}}$ generation/6$^{\text{th}}$ generation (B5G/6G) mobile communication technology (Chettri and Bera, 2020; Nguyen et al., 2022). It supports critical data harvesting from machinery sensors as well as control signaling delivery to actuators for the smart factory (Hořejší et al., 2020; Hussain et al., 2020). As an example, high-definition real-time video transmission in the IIoT provides a wide range of sensing capabilities for the smart factory, including physical-space security surveillance (Borges and Izquierdo, 2010), vision-based quality inspection (Akhyar et al., 2019), and high-precision video-based localization (Chen et al., 2017). In these cases, high-volume videos need

‡ Corresponding author

* Z. ZHENG is supported by the National Natural Science Foundation of China (No. 61901033) and the Natural Science Foundation of Beijing (No. L212031); X.Y. BAO is supported by the China Academy of Information and Communications Technology; Y.Z. HUANG is supported by the National Natural Science Foundation of China (No. 61971474) and the Beijing Nova Program (No. Z201100006820121)

ORCID: Xinyao WANG, https://orcid.org/0000-0001-5529-9554; Zhong ZHENG, https://orcid.org/0000-0002-3955-2510

to be transmitted from the sensors to the collector, which requires high-speed and secure communication links to guarantee video quality and industrial information security. In addition to the rigorous confidentiality requirement, one of the major issues that have limited massive deployments of IIoT systems is the high cost of acquiring or leasing the spectrum license.

To acquire the operation spectrum with reduced cost, the unlicensed spectrum has been introduced to IIoT systems, opportunistically exploiting airtime among other spectrum users (Hampel et al., 2019; Lu et al., 2019). Traditionally, there exist two sharing mechanisms in the unlicensed spectrum, i.e., the listen-before-talk (LBT) mode and the underlying cognitive radio (CR) mode. LBT is contention-based spectrum access and is not suitable for delay-sensitive IIoT applications. Although the underlying CR mode avoids the delay due to spectrum contention, it requires IIoT devices to restrict the radiated interference power towards the primary users (PUs).

To address both the information security and the interference mitigation issues, we resort to the cooperative multi-input multi-output (C-MIMO) transmission technique for underlaid IIoT systems. As shown in Fig. 1, several IIoT sensors inside the factory building form a cooperative cluster and jointly transmit to the remote data collector. The transmissions are subject to secrecy constraints that prevent eavesdroppers outside the building from intercepting confidential messages, and also to the interference constraint that avoids excessive interference toward PUs.

1.2 Related works

Physical layer security (PLS) techniques guarantee information security from an information-theoretic perspective, where the wireless transmission is between the legitimate transmitter (Alice) and receiver (Bob), but overheard by the eavesdropper (Eve). PLS is a classical model, where communication security is realized by proper coset coding at Alice, so that the mutual information between Alice and Eve is zero (Wyner, 1975). With this secrecy constraint, the limited information rate between Alice and Bob is represented by the secrecy capacity, which is given by the difference between the Shannon rates of wireless channels from Alice to Bob and from

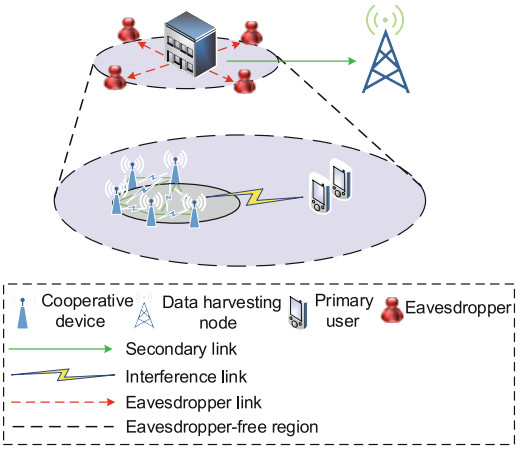

Fig. 1 Diagram of the underlaid secrecy C-MIMO with the location-constrained multiple eavesdroppers in an IIoT scenario (C-MIMO: cooperative multi-input multi-output; IIoT: Industrial Internet of Things)

Alice to Eve (Csiszar and Körner, 1978). To this end, Alice has to obtain the knowledge of both channels to adapt its coding scheme and coding rate. Therefore, the knowledge of channel state information (CSI) is crucial in designing secrecy transmissions. However, in realistic systems, a covert eavesdropper behaves as a receiver and does not transmit any signal. Alice cannot obtain the realizations of the eavesdropping channel by measuring the transmission from Eve.

To guarantee perfect secrecy with partial or no channel knowledge of Eve, artificial noise (AN) injection by Alice has been considered (Goel and Negi, 2008; Zhou and McKay, 2010; Zhu Y et al., 2013). With AN injection, the total transmit power is split between the confidential signal and the AN, and AN is transmitted in the null-space of the channel between Alice and Bob. He and Yener (2014) presented codebook construction and the related secrecy rate, where the signal and AN were superimposed in the same vector space. In Goel and Negi (2008), Zhou and McKay (2010), Zhu Y et al. (2013), and He and Yener (2014), the lower bound of the secrecy rate was obtained by ignoring the thermal noise at Eve, which is equivalent to the case in which Eve can be anywhere in the network. In some communication scenarios, this is an overly conservative assumption that leads to a pessimistic estimation of the secrecy rate. Although information security can be

guaranteed by deducing the previously referenced lower bound of the achievable secrecy rate, it sacrifices the efficiency of scarce spectrum resources in the IIoT scenario. In Zhang et al. (2013), Zheng TX et al. (2015), and Deng et al. (2016), a certain secrecy outage probability was allowed to improve the information rate at the expense of the compromised secrecy constraint. In Wang et al. (2016), the secrecy rate was evaluated for a large distributed antenna system, where Alice was composed of distributed antennas and Eve had a single fixed location known a priori. Therein, the secrecy rate maximization was recast into a max-min problem using results from the random matrix theory and solved by the iterative block coordinate descent algorithm. However, the adopted asymptotic analysis was valid only when the number of antennas at Alice, Bob, and Eve approached infinity.

In Sibomana et al. (2015), Zhu FC and Yao (2016), and Hu et al. (2018), PLS techniques were investigated for CR systems, assuming a pair of PU transceivers and a pair of secondary user transceivers coexisting with a malicious eavesdropper. Therein, the transmitters sent their own confidential messages to intended receivers in case of being overheard by eavesdroppers, and kept the mutual interference below a tolerable threshold. To this end, different interference metrics were chosen as the subjection for this secrecy rate optimization problem, e.g., the outage probability constraint for the PUs (Sibomana et al., 2015), interference power constraint for the PUs (Hu et al., 2018), and lower-bound signal-to-interference-plus-noise ratio (SINR) constraint for the PUs along with the upper-bound SINR constraint for eavesdroppers (Zhu FC and Yao, 2016). In addition, prior knowledge of CSI is crucial for PLS technology. In Pei et al. (2010), the underlaid secrecy rate for a multi-input single-output single-eavesdropper (MISOSE) wiretap channel was deduced assuming that perfect CSI of all users was known at Alice. The worst-case secrecy rate for a multi-input multi-output multi-eavesdropper (MIMOME) wiretap channel, assuming that perfect CSI of all users was known at Alice, was derived in Fang et al. (2016) and Hu et al. (2018). Previous works have focused mainly on the secrecy capacity under the perfect assumption of the eavesdropping channels, which would lead to an optimistic estimation of the secrecy rate and cause an information leakage issue in practical IIoT systems.

1.3 Our contributions

Due to the passive nature of the eavesdropping devices, only partial or no channel knowledge can be harnessed to design and optimize the considered secrecy communications of the underlaid CR systems. Specifically, a novel PLS optimization framework is investigated assuming the constrained eavesdropper's location, which potentially improves the achieved secrecy rate while leveraging the practical location constraint. To further disrupt the information received at Eve, the confidential signal and AN are jointly precoded in the eigenspace of the channel matrix and randomly superimposed at Eve, while satisfying the interference constraint at the PU. Our main contributions are summarized as follows:

1. We consider a realistic underlaid secrecy CR system, where the C-MIMO transceivers coexist with a PU and the eavesdroppers can appear at multiple possible locations in the network. This is useful to relax the "anywhere Eve" assumption adopted in other works (Goel and Negi, 2008; Zhou and McKay, 2010; Zhu Y et al., 2013; He and Yener, 2014), and the considered framework can take into account the practical constraints of the system topology. Specifically, if there exists an area around Alice guaranteed to be free of an eavesdropper, the signal and AN can be optimized assuming that Eve is outside the eavesdropper-free region and is located at an arbitrary finite number of sampled locations.

2. We propose an eigenspace-adaptive precoding (EAP) method for the underlaid C-MIMO system by jointly designing the signal and the AN. The signal and the AN are adaptively transmitted in the eigenspace of the main channel or the null-space of the interference channel according to the interference power constraint at the PU and the CSI of the legitimate channel. Depending on the selected eigenspace, the secrecy rate maximization is re-formulated as two canonical difference convex (CDC) problems, which are then solved by an iterative outer approximation algorithm, where the required average mutual information between Alice and Eve is given by closed-form approximation.

3. To adapt to the low-powered and massively populated device scenario, we simplify the EAP method by adopting uniform power allocation. Specifically, when the null-space AN injection is

considered, the original power allocation problem is simplified into a two-variable optimization problem. It is solved by an iterative power allocation algorithm from Lin et al. (2013), which achieves almost the same performance as a brute-force search with much lower complexity. When the null-space of the PU's channel is considered, the orthogonal subspace projection method is adopted to improve the information rate of the legitimate channel by aligning the sub-null-space of the PU channel with the eigenspace of the main channel, which is also solved by the iterative power allocation algorithm.

2 System model

As shown in Fig. 2, we consider a secondary C-MIMO system between K clustered transmit nodes and a receive node, where the transmit cluster has a head node at the center and the cluster radius is r. The transmit cluster is referred to as Alice and the receiver is referred to as Bob, where each transmit node is equipped with a single antenna and the receive node is equipped with N_{B} antennas. The distance between the head of Alice and Bob is denoted by b_0. The secret messages from the transmit cluster can be intercepted by Eve, which is equipped with N_{E} antenna elements ($N_{\mathrm{E}} \geq 1$) and is located outside a predefined eavesdropper-free region. In addition, we assume that a PU (PU refers to the PU receiver mentioned in the introduction, that is, the receiver of the primary user) equipped with N_{P} receive antennas at a distance of p_0 from the head of Alice can overhear the underlaid transmissions, which is regarded as an unnecessary interference toward the PU.

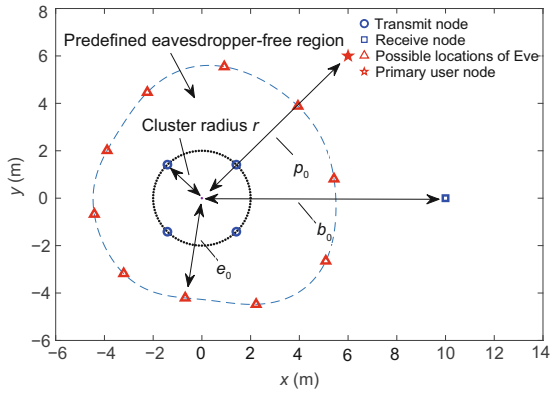

Fig. 2 Mathematical model of a C-MIMO underlaid CR system with a location-restricted region for Eve around transmitters (C-MIMO: cooperative multi-input multi-output; CR: cognitive radio). The possible locations of Eve are along the contour of the region

The transmit head node is responsible for precoding the information and conveys the encoded signals to the transmit cluster members. Similar to Zheng Z and Haas (2017), we assume that the necessary cooperation signaling is perfectly exchanged among transmitters without delay. The fundamental limit of the information rate between the transmit cluster and the receiver is given by the Shannon rate of the distributed MIMO channel (Ozgur et al., 2013). In addition, we focus on the physical layer security of the communication between Alice and Bob, while we assume that the security of the intra-cluster cooperation within Alice can be guaranteed relatively easily. This is because the communication links have a shorter range and therefore could provide higher channel capacity.

2.1 Channel model

Consider a transmit vector $\boldsymbol{x} = [x_1, x_2, \ldots, x_K]^{\mathrm{T}}$, where x_k ($k = 1, 2, \ldots, K$) denotes the transmitted symbol from the k^{th} transmit node of Alice. The receive vectors of Bob, PU, and Eve at the i^{th} location are denoted as $\boldsymbol{y} = [y_1, y_2, \ldots, y_{N_{\mathrm{B}}}]^{\mathrm{T}}$, $\boldsymbol{u} = [u_1, u_2, \ldots, u_{N_{\mathrm{P}}}]^{\mathrm{T}}$, and $\boldsymbol{z}_i = [z_{i,1}, z_{i,2}, \ldots, z_{i,N_{\mathrm{E}}}]^{\mathrm{T}}$, respectively, where y_n, u_n, and $z_{i,n}$ denote the receive symbols at the n^{th} receive antenna of Bob, PU, and the i^{th} Eve, respectively. The vectors $\boldsymbol{y}$, $\boldsymbol{u}$, and $\boldsymbol{z}_i$ are expressed as

$$\boldsymbol{y} = \boldsymbol{H}\,\boldsymbol{x} + \boldsymbol{n}_{\mathrm{B}}, \tag{1}$$

$$\boldsymbol{u} = \boldsymbol{G}\,\boldsymbol{x} + \boldsymbol{n}_{\mathrm{P}}, \tag{2}$$

$$\boldsymbol{z}_i = \boldsymbol{F}_i\,\boldsymbol{x} + \boldsymbol{n}_{\mathrm{E}},\ 1 \leq i \leq L, \tag{3}$$

where L is the number of possible locations of Eve. The matrix entry $H_{n,k}$ on the n^{th} row and k^{th} column of $\boldsymbol{H}$ denotes the channel coefficient between the k^{th} transmitter and the n^{th} receiver, i.e., $\boldsymbol{H} \in \mathbb{C}^{N_{\mathrm{B}} \times K}$, similarly, $\boldsymbol{G} \in \mathbb{C}^{N_{\mathrm{P}} \times K}$ and $\boldsymbol{F}_i \in \mathbb{C}^{N_{\mathrm{E}} \times K}$. As the antenna elements at Bob are co-located, the legitimate channel between Alice and Bob can be written as

$$\boldsymbol{H} = \boldsymbol{L}\boldsymbol{\Omega}^{1/2}, \tag{4}$$

where $\boldsymbol{L}$ denotes the fast fading coefficients, modeled as an independent and identically distributed (i.i.d.) standard complex Gaussian random matrix,

i.e., $\boldsymbol{L} \sim \mathcal{CN}(\boldsymbol{0}, \boldsymbol{I})$. The $K \times K$ diagonal matrix $\boldsymbol{\Omega} = \mathrm{diag}(\omega_1, \omega_2, \ldots, \omega_K)$ denotes the average channel gains with the k^{th} diagonal entry being

$$\omega_k = c_{\mathrm{p}} b_k^{-\alpha}, \tag{5}$$

where b_k denotes the distance between the k^{th} transmitter of Alice and Bob, α is the path-loss exponent, and c_{p} is the path loss at the unit distance. Similarly, the channel between Alice and Eve at the i^{th} location can be written as

$$\boldsymbol{F}_i = \boldsymbol{W}_i \boldsymbol{\Sigma}_i^{1/2}, \tag{6}$$

where $\boldsymbol{W}_i \sim \mathcal{CN}(\boldsymbol{0}, \boldsymbol{I})$. The $K \times K$ diagonal matrix $\boldsymbol{\Sigma}_i = \mathrm{diag}(\sigma_{i,1}, \sigma_{i,2}, \ldots, \sigma_{i,K})$ denotes the average channel gains with the k^{th} diagonal entry being

$$\sigma_{i,k} = c_{\mathrm{p}} e_{i,k}^{-\alpha}, \tag{7}$$

where $e_{i,k}$ denotes the distance between the k^{th} transmitter and the i^{th} Eve. The channel matrix between Alice and the PU is represented as

$$\boldsymbol{G} = \boldsymbol{M} \boldsymbol{\Theta}^{1/2}, \tag{8}$$

where $\boldsymbol{M}$ is a standard complex Gaussian random matrix and the diagonal matrix $\boldsymbol{\Theta} = \mathrm{diag}(\theta_1, \theta_2, \ldots, \theta_K)$ denotes the average channel gains with the k^{th} diagonal entry being

$$\theta_k = c_{\mathrm{p}} p_k^{-\alpha}, \tag{9}$$

where p_k denotes the distance between the k^{th} transmitter and the PU. In addition, c_{p} and α are assumed to be the same as those of Eve's channel. The additive noises $\boldsymbol{n}_{\mathrm{B}}$, $\boldsymbol{n}_{\mathrm{P}}$, and $\boldsymbol{n}_{\mathrm{E}}$ at Bob, PU, and Eve are modeled as i.i.d. complex Gaussian vectors with normalized power, i.e., $\boldsymbol{n}_{\mathrm{B}} \sim \mathcal{CN}(\boldsymbol{0}, \boldsymbol{I}_{N_{\mathrm{B}}})$, $\boldsymbol{n}_{\mathrm{P}} \sim \mathcal{CN}(\boldsymbol{0}, \boldsymbol{I}_{N_{\mathrm{P}}})$, and $\boldsymbol{n}_{\mathrm{E}} \sim \mathcal{CN}(\boldsymbol{0}, \boldsymbol{I}_{N_{\mathrm{E}}})$. In this study, we assume that $\boldsymbol{H}$, $\boldsymbol{F}_i$, and $\boldsymbol{G}$ all follow block fading processes. In addition, the instantaneous CSI of $\boldsymbol{H}$ is known by Alice and Bob, while the instantaneous CSI of $\boldsymbol{G}$ is known by Alice and the PU. However, only the statistical CSI of $\boldsymbol{F}_i$, depending on the number of receive antennas at Eve and the location of Eve, could be acquired by Alice by evaluating the worst-case scenario; i.e., N_{E} is set to the maximum number of antennas allowed at Eve and Eve's locations are along the contour of the eavesdropper-free region, as shown in Fig. 2.

2.2 Signal model with artificial noise injection

The wiretap channel (Eqs. (1)–(3)) with multiple possible locations of Eve can be modeled as the compound wiretap channel (Bloch and Laneman, 2013). With CSI available at the receivers, the following secrecy rate is achievable:

$$\max_{p(\boldsymbol{x})} [I(\boldsymbol{x}; \boldsymbol{y}, \boldsymbol{H}) - \max_{1 \le i \le L} I(\boldsymbol{x}; \boldsymbol{z}_i, \boldsymbol{F}_i)]^+, \tag{10}$$

where $[x]^+ = x$ for $x \ge 0$ and 0 otherwise. We denote $I(a; b_1, b_2)$ as the mutual information between the random variable a and the random variables b_1, b_2. The outer optimization in Eq. (10) is taken over $p(\boldsymbol{x})$, the probability distribution of $\boldsymbol{x}$. By following similar arguments in Lin et al. (2013), the mutual information $I(\boldsymbol{x}; \boldsymbol{z}_i, \boldsymbol{F}_i)$ is calculated as

$$I(\boldsymbol{x}; \boldsymbol{z}_i, \boldsymbol{F}_i) = I(\boldsymbol{x}; \boldsymbol{z}_i | \boldsymbol{F}_i) + I(\boldsymbol{x}; \boldsymbol{F}_i) = I(\boldsymbol{x}; \boldsymbol{z}_i | \boldsymbol{F}_i), \tag{11}$$

where the first equality is due to the chain rule of mutual information, and the second equality is obtained because the block fading channel $\boldsymbol{F}_i$ is independent of $\boldsymbol{x}$.

To achieve rate maximization through optimizing the probability distribution $p(\boldsymbol{x})$ is still an open problem for generic MIMO wiretap channels. To proceed, we adopt the widely used Gaussian signaling applied in other works (Goel and Negi, 2008; Zhou and McKay, 2010; Zhang et al., 2013; Zhu Y et al., 2013; He and Yener, 2014; Zheng TX et al., 2015; Wang et al., 2016), where $\boldsymbol{x}$ is a multivariate Gaussian vector. In addition, to obscure the information reception by Eve, AN is injected by Alice along with the information symbols. The transmitted symbol $\boldsymbol{x}$ is the sum of the precoded information and AN, i.e.,

$$\boldsymbol{x} = \boldsymbol{V}_{\mathrm{s}} \boldsymbol{\Psi}_{\mathrm{s}}^{1/2} \boldsymbol{s} + \boldsymbol{V}_{\mathrm{a}} \boldsymbol{\Psi}_{\mathrm{a}}^{1/2} \boldsymbol{a}, \tag{12}$$

where $\boldsymbol{s} \sim \mathcal{CN}(\boldsymbol{0}, \boldsymbol{I}_K)$ and $\boldsymbol{a} \sim \mathcal{CN}(\boldsymbol{0}, \boldsymbol{I}_K)$ are the information symbols and AN, respectively. The nonnegative diagonal matrix $\boldsymbol{\Psi}_x \succeq \boldsymbol{0}$ ($x \in \{\mathrm{s}, \mathrm{a}\}$) denotes the power allocation, where the k^{th} diagonal element $\psi_{x,k} \ge 0$ is the power allocated to the k^{th} transmit antenna. Moreover, to reflect the low-power characteristic of the considered IIoT scene, we set $0 \le \Psi_{\mathrm{p}}^{[kk]} \le \Gamma_{\mathrm{s}}$ ($k = 1, 2, \ldots, K$), where $\boldsymbol{\Psi}_{\mathrm{p}} = \boldsymbol{V}_{\mathrm{s}} \boldsymbol{\Psi}_{\mathrm{s}} \boldsymbol{V}_{\mathrm{s}}^{\dagger} + \boldsymbol{V}_{\mathrm{a}} \boldsymbol{\Psi}_{\mathrm{a}} \boldsymbol{V}_{\mathrm{a}}^{\dagger}$ ($\dagger$ denotes the conjugate transpose operation for a matrix) and Γ_{s} denotes the maximum transmit power of a single antenna. The spatial precoding matrix $\boldsymbol{V}_x$ ($x \in \{\mathrm{s}, \mathrm{a}\}$) maps the

symbols to the transmit antennas. To improve the worst-case secrecy rate under the constraint of the total power at Alice and the interference power at the PU, we design the transmit signal to be able to flexibly choose the underlying eigenspace according to the problem constraints, i.e., the EAP method, where the precoder is selected from the following two sets of eigenvectors:

1. Eigenspace precoding $\boldsymbol{V}_{\mathrm{H}}$

Let $\boldsymbol{V}_{\mathrm{s}}=\boldsymbol{V}_{\mathrm{a}}=\boldsymbol{V}_{\mathrm{H}}$ and the columns of $\boldsymbol{V}_{\mathrm{H}}$ are the right singular vectors of the main channel $\boldsymbol{H}$; i.e., $\boldsymbol{H}$ has the singular value decomposition $\boldsymbol{H}=\boldsymbol{U}_{\mathrm{H}}\boldsymbol{\Lambda}_{\mathrm{H}}^{1/2}\boldsymbol{V}_{\mathrm{H}}^{\dagger}$. Note that the null-space AN injection in other works (Goel and Negi, 2008; Zhou and McKay, 2010; Zhang et al., 2013; Zhu Y et al., 2013; Zheng TX et al., 2015) can be viewed as a special case of Eq. (12), where $\boldsymbol{V}_{\mathrm{s}}$ and $\boldsymbol{V}_{\mathrm{a}}$ are chosen as the orthogonal sub-spaces of $\boldsymbol{V}_{\mathrm{H}}$, i.e., $\boldsymbol{V}_{\mathrm{s}}^{\dagger}\boldsymbol{V}_{\mathrm{a}}=\boldsymbol{0}$. Therefore, the precoder structure (Eq. (12)) is more general than the null-space AN injection, which can be realized by Eq. (12) by properly setting the power allocation variables $\psi_{x,k}=0$.

2. Null-space precoding $\boldsymbol{V}_{\mathrm{G}}$

To avoid the interference toward the PU, the signal and AN can be precoded in the null-space of the interference channel $\boldsymbol{G}$, i.e., $\boldsymbol{V}_{\mathrm{s}}=\boldsymbol{V}_{\mathrm{a}}=\boldsymbol{V}_{\mathrm{G}}$, where $\boldsymbol{G}\boldsymbol{V}_{\mathrm{G}}=\boldsymbol{0}$. The columns of $\boldsymbol{V}_{\mathrm{G}}$ can be selected as the right singular vectors of the interference channel corresponding to the zero singular values. Note that this precoding scheme further requires that the number of transmitters be larger than the number of antennas at the PU, i.e., $K\geq N_{\mathrm{P}}$.

Accordingly, following the above two eigenvector precoding schemes, the transmit signal of the proposed EAP can be written as

$$\boldsymbol{x}=\tilde{\boldsymbol{V}}\boldsymbol{S}\boldsymbol{\Psi}_{\mathrm{s}}^{1/2}\boldsymbol{s}+\tilde{\boldsymbol{V}}\boldsymbol{S}\boldsymbol{\Psi}_{\mathrm{a}}^{1/2}\boldsymbol{a}, \tag{13}$$

where $\tilde{\boldsymbol{V}}=[\boldsymbol{V}_{\mathrm{H}},\boldsymbol{V}_{\mathrm{G}}]$, and $\boldsymbol{S}$ is an eigenspace selector and is denoted as

$$\boldsymbol{S}=\begin{cases}\begin{bmatrix}\boldsymbol{I}_{K\times K} & \boldsymbol{0}_{K\times r}\end{bmatrix}^{\mathrm{T}}, & \text{if } \boldsymbol{V}_{\mathrm{H}} \text{ is selected},\\ \begin{bmatrix}\boldsymbol{0}_{r\times K} & \boldsymbol{I}_{r\times r}\end{bmatrix}^{\mathrm{T}}, & \text{if } \boldsymbol{V}_{\mathrm{G}} \text{ is selected},\end{cases} \tag{14}$$

where r denotes the number of zero singular values of the interference channel $\boldsymbol{G}$. According to Eq. (13), we can improve the secrecy rate of the underlaid secrecy CR system by jointly optimizing the power allocation vectors and the eigenspace selector. The eigenspace selection will be specifically discussed in Section 3.2.

2.3 Problem formulation

According to Eq. (10), the secrecy rate under a pair of fixed $\boldsymbol{\Psi}_{\mathrm{s}}$ and $\boldsymbol{\Psi}_{\mathrm{a}}$ can be explicitly written as

$$\begin{aligned}R_{\mathrm{s}}(\boldsymbol{S},\boldsymbol{\Psi}_{\mathrm{s}},\boldsymbol{\Psi}_{\mathrm{a}})=&R_{\mathrm{B}}(\boldsymbol{S},\boldsymbol{\Psi}_{\mathrm{s}},\boldsymbol{\Psi}_{\mathrm{a}})\\&-\max_{1\leq i\leq L}R_{\mathrm{E},i}(\boldsymbol{S},\boldsymbol{\Psi}_{\mathrm{s}},\boldsymbol{\Psi}_{\mathrm{a}}),\end{aligned} \tag{15}$$

where R_{B} and $R_{\mathrm{E},i}$ are the information rates of the main and the i^{th} eavesdropping channel, respectively. As the main channel (Eq. (1)) and the eavesdropping channel (Eq. (3)) are Gaussian MIMO channels, these information rates with AN injection follow the well-known MIMO channel capacity in Chiurtu et al. (2001) as

$$R_{\mathrm{B}}(\boldsymbol{S},\boldsymbol{\Psi}_{\mathrm{s}},\boldsymbol{\Psi}_{\mathrm{a}})=f_{\mathrm{B}}(\boldsymbol{S},\boldsymbol{\Psi}_{\mathrm{s}}+\boldsymbol{\Psi}_{\mathrm{a}})-f_{\mathrm{B}}(\boldsymbol{S},\boldsymbol{\Psi}_{\mathrm{a}}), \tag{16}$$

$$R_{\mathrm{E},i}(\boldsymbol{S},\boldsymbol{\Psi}_{\mathrm{s}},\boldsymbol{\Psi}_{\mathrm{a}})=f_{\mathrm{E},i}(\boldsymbol{S},\boldsymbol{\Psi}_{\mathrm{s}}+\boldsymbol{\Psi}_{\mathrm{a}})-f_{\mathrm{E},i}(\boldsymbol{S},\boldsymbol{\Psi}_{\mathrm{a}}). \tag{17}$$

By denoting $\boldsymbol{X}$ as a multi-column selection matrix and $\boldsymbol{Y}$ as a $K\times K$ positive semi-definite Hermitian matrix, the information rate of Bob (f_{B}) and that of Eve ($f_{\mathrm{E},i}$) are separately defined as

$$f_{\mathrm{B}}(\boldsymbol{X},\boldsymbol{Y})=\log_2\det\left(\boldsymbol{I}+\boldsymbol{V}_{\mathrm{H}}\boldsymbol{\Lambda}_{\mathrm{H}}\boldsymbol{V}_{\mathrm{H}}^{\dagger}\tilde{\boldsymbol{V}}\boldsymbol{X}\boldsymbol{Y}\boldsymbol{X}^{\dagger}\tilde{\boldsymbol{V}}^{\dagger}\right), \tag{18}$$

$$\begin{aligned}&f_{\mathrm{E},i}(\boldsymbol{X},\boldsymbol{Y})\\=&\mathbb{E}\left[\log_2\det\left(\boldsymbol{I}+\boldsymbol{W}_i\boldsymbol{\Sigma}_i^{1/2}\tilde{\boldsymbol{V}}\boldsymbol{X}\boldsymbol{Y}\boldsymbol{X}^{\dagger}\tilde{\boldsymbol{V}}^{\dagger}\boldsymbol{\Sigma}_i^{1/2}\boldsymbol{W}_i^{\dagger}\right)\right].\end{aligned} \tag{19}$$

To balance the underlaid secrecy rate and the interference at the PU, the objective function is designed to maximize the worst-case secrecy rate in the underlaid communication system while subject to both the total power constraint at Alice and the interference power constraint at the PU. We optimize the worst-case underlaid secrecy rate by jointly optimizing the power allocation vectors of information symbols and AN, and the eigenspace selector of the precoder, i.e., $\{\boldsymbol{S},\boldsymbol{\Psi}_{\mathrm{s}},\boldsymbol{\Psi}_{\mathrm{a}}\}$. Accordingly, the optimization problem in our proposed underlaid secrecy CR network can be written as

$$\max_{\boldsymbol{S},\boldsymbol{\Psi}_{\mathrm{s}}\succeq\boldsymbol{0},\boldsymbol{\Psi}_{\mathrm{a}}\succeq\boldsymbol{0}}[R_{\mathrm{s}}(\boldsymbol{S},\boldsymbol{\Psi}_{\mathrm{s}},\boldsymbol{\Psi}_{\mathrm{a}})]^{+} \tag{20a}$$

$$\text{s.t. } 0\leq\Psi_{\mathrm{p}}^{[kk]}\leq\Gamma_{\mathrm{s}},\ k=1,2,\ldots,K, \tag{20b}$$

$$0\leq\mathrm{tr}\left(\boldsymbol{G}\tilde{\boldsymbol{V}}\boldsymbol{S}(\boldsymbol{\Psi}_{\mathrm{s}}+\boldsymbol{\Psi}_{\mathrm{a}})\boldsymbol{S}^{\dagger}\tilde{\boldsymbol{V}}^{\dagger}\boldsymbol{G}^{\dagger}\right)\leq\Gamma_{\mathrm{I}}, \tag{20c}$$

where $\boldsymbol{\Psi}_{\mathrm{p}}=\tilde{\boldsymbol{V}}\boldsymbol{S}(\boldsymbol{\Psi}_{\mathrm{s}}+\boldsymbol{\Psi}_{\mathrm{a}})\boldsymbol{S}^{\dagger}\tilde{\boldsymbol{V}}^{\dagger}$ and $\mathrm{tr}(\cdot)$ denotes the trace of a matrix. Constraint (20b) is due to the maximum transmit power Γ_{s} of a single antenna imposed by Alice, and constraint (20c) is due to the fact that the maximum interference received at the PU should be below a given threshold Γ_{I}.

Compared with Eq. (10), the secrecy rate (Eq. (20)) is suboptimal due to the Gaussian signaling and the specific precoder structure (Eq. (13)). However, optimization problem (20) can be solved relatively easily and the numerical results in Section 6 will show that substantial secrecy rates can still be achieved. In the next section, we present an approximate closed-form expression for the average rates $R_{\mathrm{E},i}$ and the optimization framework to solve problem (20).

3 Secrecy rate maximization under eigenspace-adaptive precoding

3.1 Approximation of the ergodic information rate for eavesdropping channels

In the literature, the function $f_{\mathrm{E}}(\boldsymbol{\Psi})$ is the ergodic capacity of Rayleigh MIMO channels with transmitter-side correlation $\boldsymbol{T}=\boldsymbol{\Sigma}^{1/2}\tilde{\boldsymbol{V}}\boldsymbol{S}\boldsymbol{\Psi}\boldsymbol{S}^{\dagger}\tilde{\boldsymbol{V}}^{\dagger}\boldsymbol{\Sigma}^{1/2}$. Note that we ignore the subindex i whenever it is clear from the context. The expression of $f_{\mathrm{E}}(\boldsymbol{\Psi})$ (e.g., Eq. (123) in Simon et al. (2006)) depends on the eigenvalues of $\boldsymbol{T}$. For a matrix with arbitrary dimension, there does not exist a closed-form expression of its eigenvalues, so one must resort to numerical and iterative routines. When $f_{\mathrm{E}}(\cdot)$ is used in optimization problem (20), the relevant algorithm typically starts from an initial value $\boldsymbol{T}_0$ and approaches the optimal solution via a sequence of iterations, saying $\boldsymbol{T}_1,\boldsymbol{T}_2,\ldots,\boldsymbol{T}_{\mathrm{a}}$. Therefore, one must calculate all the eigenvalues of $\boldsymbol{T}_0,\boldsymbol{T}_1,\ldots,\boldsymbol{T}_{\mathrm{a}}$, which requires prohibitively more computational resources.

To address this issue, we approximate the information rate between Alice and Eve as

$$\begin{aligned}R_{\mathrm{E}}(\boldsymbol{\Psi}_{\mathrm{s}},\boldsymbol{\Psi}_{\mathrm{a}})&\approx\widetilde{R}_{\mathrm{E}}(\boldsymbol{\Psi}_{\mathrm{s}},\boldsymbol{\Psi}_{\mathrm{a}})\\&=\widetilde{f}_{\mathrm{E}}(\boldsymbol{\Psi}_{\mathrm{s}}+\boldsymbol{\Psi}_{\mathrm{a}})-\widetilde{f}_{\mathrm{E}}(\boldsymbol{\Psi}_{\mathrm{a}}),\end{aligned}\tag{21}$$

where

$$\widetilde{f}_{\mathrm{E}}(\boldsymbol{Z})=\log_2\mathbb{E}\left[\det\left(\boldsymbol{I}+\boldsymbol{W}\boldsymbol{\Sigma}^{1/2}\boldsymbol{\Phi}\boldsymbol{Z}\boldsymbol{\Phi}^{\dagger}\boldsymbol{\Sigma}^{1/2}\boldsymbol{W}^{\dagger}\right)\right].\tag{22}$$

Here, $\boldsymbol{Z}$ is a diagonal matrix, $\boldsymbol{\Phi}$ is a random unitary matrix, and each instance of $\boldsymbol{\Phi}$ is drawn uniformly and randomly from the Haar measure (Sternberg, 1995). The expectation in Eq. (22) is taken over both $\boldsymbol{W}$ and $\boldsymbol{\Phi}$. Comparing $\widetilde{f}_{\mathrm{E}}(\cdot)$ with $f_{\mathrm{E}}(\cdot)$ in Eq. (19), we replace the unitary matrix $\tilde{\boldsymbol{V}}$ with a random Haar unitary matrix $\boldsymbol{\Phi}$, and apply Jensen's inequality.

Denoting $\{\mathcal{M}_{i,j}\}_{1\le i\le a,1\le j\le b}$ as an $a\times b$ matrix block, we define the $a\times a$ Vandermonde matrix as $\boldsymbol{M}=[\{m_i^{j-1}\}_{1\le i,j\le a}]$. Its determinant is calculated as $\Delta_a(\boldsymbol{m})=\det[\boldsymbol{M}]=\prod_{1\le i<j\le a}(m_j-m_i)$. The following two propositions present closed-form expressions of $\exp(\widetilde{f}_{\mathrm{E}}(\boldsymbol{Z}))$, where the proofs rely on the group integrals over the Haar unitary matrix $\boldsymbol{\Phi}$. We omit the proofs here and refer the readers to Zheng Z et al. (2019) for detailed derivations.

Proposition 1 Let $z_1,z_2,\ldots,z_n>0$ and $z_{n+1}=z_{n+2}=\ldots=z_K=0$. When $M\ge K\ge n$, $\exp(\widetilde{f}_{\mathrm{E}}(\boldsymbol{Z}))$ is given as

$$\begin{aligned}&\exp\left(\widetilde{f}_{\mathrm{E}}(\boldsymbol{Z})\right)=\\&\frac{\prod_{i=1}^{n}z_i^{n-K}}{\Delta_K(\boldsymbol{\sigma})\Delta_n(\boldsymbol{z})}\det\begin{bmatrix}\{\sigma_j^{i-1}\}_{\substack{1\le i\le K-n\\1\le j\le K}}\\\{\mathcal{J}_{i,j}\}_{\substack{1\le i\le n\\1\le j\le K}}\end{bmatrix}\\&\cdot\prod_{j=K-n}^{K-1}\frac{\Gamma(K+1-j)\Gamma(j+1)(M-K)!}{\Gamma(M-K+j+1)K!},\end{aligned}\tag{23}$$

where $\mathcal{J}_{i,j}=\sum_{l=0}^{K}\dfrac{\Gamma(M-K+1+l)\Gamma(K+1)(z_i\sigma_j)^l}{\Gamma(M-K+1)\Gamma(K+1-l)\Gamma(l+1)}$.

Proposition 2 Let $z_1,z_2,\ldots,z_n>0$ and $z_{n+1}=z_{n+2}=\ldots=z_K=0$. When $K>M\ge n$, $\exp(\widetilde{f}_{\mathrm{E}}(\boldsymbol{Z}))$ is given as

$$\begin{aligned}&\exp\left(\widetilde{f}_{\mathrm{E}}(\boldsymbol{Z})\right)=\\&\frac{\prod_{i=1}^{n}z_i^{n-M}}{\Delta_K(\boldsymbol{\sigma})\Delta_n(\boldsymbol{z})}\det\begin{bmatrix}\{\sigma_j^{i-1}\}_{\substack{1\le i\le K-n\\1\le j\le K}}\\\{\sigma_j^{K-M}\mathcal{K}_{i,j}\}_{\substack{1\le i\le n\\1\le j\le K}}\end{bmatrix}\\&\cdot\prod_{j=K-n}^{K-1}\frac{\Gamma(K+1-j)\Gamma(j+1)}{\Gamma(M-K+j+1)(K-M)!M!},\end{aligned}\tag{24}$$

where $\mathcal{K}_{i,j}=\sum_{l=0}^{M}\dfrac{\Gamma(l+1)\Gamma(M+1)\Gamma(K-M+1)(z_i\sigma_j)^l}{\Gamma(K-M+1+l)\Gamma(M+1-l)}$.

When $K > n > M$, $\exp(\widetilde{f}_{\mathrm{E}}(\boldsymbol{X}))$ is given as

$$\exp\left(\widetilde{f}_{\mathrm{E}}(\boldsymbol{Z})\right) = \frac{(-1)^{(n-M)(K-M)}}{\Delta_K(\boldsymbol{\sigma})\Delta_n(\boldsymbol{z})} \cdot \det\begin{bmatrix} \{0\}_{\substack{1\le i\le K-M\\ 1\le j\le n-M}} & \left\{\sigma_j^{i-1}\right\}_{\substack{1\le i\le K-M\\ 1\le j\le K}} \\ \left\{z_i^{j-1}\right\}_{\substack{1\le i\le n\\ 1\le j\le n-M}} & \left\{z_i^{n-M}\sigma_j^{K-M}\mathcal{K}_{i,j}\right\}_{\substack{1\le i\le n\\ 1\le j\le K}} \end{bmatrix} \cdot \prod_{j=n-M}^{n-1} \frac{\Gamma(n+1-j)\Gamma(K-n+j+1)}{\Gamma(M-n+j+1)(K-M)!M!}. \tag{25}$$

Fig. 3 compares the approximate mutual information $\widetilde{R}_{\mathrm{E},i}$ between Alice and the i^{th} Eve calculated in Eq. (21) with the exact mutual information $R_{\mathrm{E},i}$ in Eq. (17) with $K = N = 4$ and $M = 2$, using randomly chosen power allocations $\boldsymbol{\Psi}_{\mathrm{s}}$ and $\boldsymbol{\Psi}_{\mathrm{a}}$. The locations of transmitters are as shown in Fig. 2 and the location of the i^{th} Eve is set to $(e_i, 0)$. By increasing the cluster radius r, the radial distances of the transmitters are proportionally increased. We generate 10^4 realizations of the precoding matrix $\boldsymbol{V}_{\mathrm{H}}$, and plot one standard deviation above and below the expectation of $R_{\mathrm{E},i}$ averaged over $\boldsymbol{V}_{\mathrm{H}}$. Fig. 3 shows that approximation (21) tends to over-estimate the exact rate $R_{\mathrm{E},i}$, which is favorable in the context of secrecy communications because it prevents setting a code rate higher than the achievable rate obtained by Eq. (20). Additionally, because the legitimate channel given by Eq. (4) and the PU channel given by Eq. (8) have the same formulation, the numerical simulations of the exact rate $R_{\mathrm{E},i}$ by using the precoder $\boldsymbol{V}_{\mathrm{G}}$ are therefore identical to those of $R_{\mathrm{E},i}$ by using the precoding $\boldsymbol{V}_{\mathrm{H}}$, if these two channels have the same configuration. Therefore, we omit the comparison between $R_{\mathrm{E},i}$ achieved by the $\boldsymbol{V}_{\mathrm{G}}$ precoding and $\widetilde{R}_{\mathrm{E},i}$.

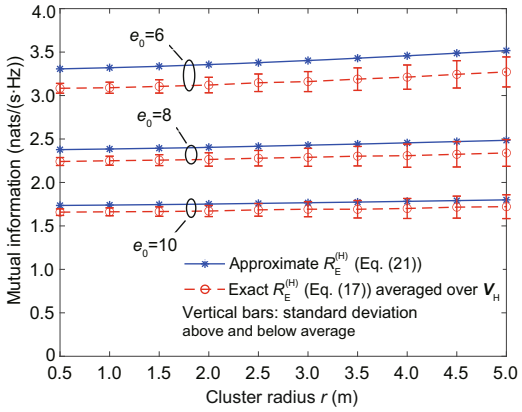

Fig. 3 Comparison of approximation (21) with Eq. (17) using randomly generated power allocations $\boldsymbol{\Psi}_{\mathrm{s}}$ and $\boldsymbol{\Psi}_{\mathrm{a}}$

3.2 Eigenspace-adaptive precoding architecture and the decomposed problem formulation

According to Eq. (22), the information rate of the wiretap channel is approximated by substituting the channel eigenspace vector $\boldsymbol{V}_x$ by a random unitary matrix $\boldsymbol{\Phi}$; thus, the precoders $\boldsymbol{V}_{\mathrm{H}}$ and $\boldsymbol{V}_{\mathrm{G}}$ can achieve the same approximated information rate at the eavesdroppers. Accordingly, substituting $R_{\mathrm{E},i}$ in Eq. (15) by Eq. (21), it is observed that the secrecy rate R_{s} of the C-MIMO system achieved by precoders $\boldsymbol{V}_{\mathrm{H}}$ and $\boldsymbol{V}_{\mathrm{G}}$ can be simply analyzed by only comparing the R_{B} achieved by the $\boldsymbol{V}_{\mathrm{H}}$ and $\boldsymbol{V}_{\mathrm{G}}$ precoding methods.

Inspired by the observations above, we propose an EAP architecture, in which the original optimization problem (20) is decomposed into two sub-problems, i.e., the optimization of eigenspace selector $\boldsymbol{S}$ and the optimization of the power allocation vectors $\{\boldsymbol{\Psi}_{\mathrm{s}}, \boldsymbol{\Psi}_{\mathrm{a}}\}$. First, we solve the $\boldsymbol{S}$-optimizing sub-problem by fixing $\boldsymbol{\Psi}_{\mathrm{s}}$ and $\boldsymbol{\Psi}_{\mathrm{a}}$. Herein, $\boldsymbol{\Psi}_{\mathrm{a}} = \boldsymbol{0}$ and $\boldsymbol{\Psi}_{\mathrm{s}} = \boldsymbol{\Psi}_{\mathrm{wf}}$ are given, where $\boldsymbol{\Psi}_{\mathrm{wf}}$ is the solution of the water-filling power allocation algorithm by optimizing $\boldsymbol{\Psi}_{\mathrm{s}}$ in R_{B} only, i.e., $\boldsymbol{\Psi}_{\mathrm{wf}} = \arg\max_{\boldsymbol{\Psi}_{\mathrm{s}}\succeq\boldsymbol{0}} R_{\mathrm{B}}(\boldsymbol{S}, \boldsymbol{\Psi}_{\mathrm{s}}, \boldsymbol{0})$, subject to $\mathrm{tr}(\boldsymbol{\Psi}_{\mathrm{s}}) \le \Gamma_{\mathrm{s}}$. Therefore, the $\boldsymbol{S}$-optimizing sub-problem can be written as

$$\max_{\boldsymbol{S}} [R_{\mathrm{B}}(\boldsymbol{S}, \boldsymbol{\Psi}_{\mathrm{s}}, \boldsymbol{\Psi}_{\mathrm{a}})]^+ \tag{26a}$$

$$\text{s.t. } 0 \le \mathrm{tr}\left(\boldsymbol{G}\tilde{\boldsymbol{V}}\boldsymbol{S}(\boldsymbol{\Psi}_{\mathrm{s}} + \boldsymbol{\Psi}_{\mathrm{a}})\boldsymbol{S}^{\dagger}\tilde{\boldsymbol{V}}^{\dagger}\boldsymbol{G}^{\dagger}\right) \le \Gamma_{\mathrm{I}}. \tag{26b}$$

It is clear that sub-problem (26) can be simply solved via comparing $R_{\mathrm{B}}^{(\mathrm{H})}$ and $R_{\mathrm{B}}^{(\mathrm{G})}$ calculated through Eq. (16) using the precoders $\boldsymbol{V}_{\mathrm{H}}$ and $\boldsymbol{V}_{\mathrm{G}}$. Specifically, if $R_{\mathrm{B}}^{(\mathrm{H})} \ge R_{\mathrm{B}}^{(\mathrm{G})}$, which shows that the eigenspace precoding $\boldsymbol{V}_{\mathrm{H}}$ outperforms the eigenspace precoding $\boldsymbol{V}_{\mathrm{G}}$ in terms of the secrecy rate, $\boldsymbol{S} = \begin{bmatrix} \boldsymbol{I}_{K\times K} & \boldsymbol{0}_{K\times r} \end{bmatrix}^{\mathrm{T}}$ should be selected; otherwise, $\boldsymbol{S} = \begin{bmatrix} \boldsymbol{0}_{r\times K} & \boldsymbol{I}_{r\times r} \end{bmatrix}^{\mathrm{T}}$ should be selected.

Second, the $\{\boldsymbol{\Psi}_{\mathrm{s}}, \boldsymbol{\Psi}_{\mathrm{a}}\}$-optimizing sub-problem is optimized by fixing $\boldsymbol{S}$, which can be re-formulated as two different sub-problems according to the selected $\boldsymbol{S}$. When $\boldsymbol{S} = \begin{bmatrix} \boldsymbol{I}_{K\times K} & \boldsymbol{0}_{K\times r} \end{bmatrix}^{\mathrm{T}}$, i.e., $\tilde{\boldsymbol{V}} = \boldsymbol{V}_{\mathrm{H}}$, by following Eq. (15), the secrecy rate under a pair of

fixed $\boldsymbol{\Psi}_{\mathrm{s}}$ and $\boldsymbol{\Psi}_{\mathrm{a}}$ can be explicitly written as

$$R_{\mathrm{s}}^{(\mathrm{H})}(\boldsymbol{\Psi}_{\mathrm{s}},\boldsymbol{\Psi}_{\mathrm{a}})=R_{\mathrm{B}}^{(\mathrm{H})}(\boldsymbol{\Psi}_{\mathrm{s}},\boldsymbol{\Psi}_{\mathrm{a}})-\max_{1\le i\le L}R_{\mathrm{E},i}^{(\mathrm{H})}(\boldsymbol{\Psi}_{\mathrm{s}},\boldsymbol{\Psi}_{\mathrm{a}}),\tag{27}$$

where the superscript (H) highlights that the precoder aligns with the eigenspace of the main channel $\boldsymbol{V}_{\mathrm{H}}$, and $R_{\mathrm{B}}^{(\mathrm{H})}$ and $R_{\mathrm{E},i}^{(\mathrm{H})}$ are the information rates of the main and eavesdropping channels under $\boldsymbol{V}_{\mathrm{H}}$, respectively. According to Eqs. (16) and (17), the information rate with AN injection under $\boldsymbol{V}_{\mathrm{H}}$ can be written as

$$R_{\mathrm{B}}^{(\mathrm{H})}(\boldsymbol{\Psi}_{\mathrm{s}},\boldsymbol{\Psi}_{\mathrm{a}})=f_{\mathrm{B}}^{(\mathrm{H})}(\boldsymbol{\Psi}_{\mathrm{s}}+\boldsymbol{\Psi}_{\mathrm{a}})-f_{\mathrm{B}}^{(\mathrm{H})}(\boldsymbol{\Psi}_{\mathrm{a}}),\tag{28}$$

$$R_{\mathrm{E},i}^{(\mathrm{H})}(\boldsymbol{\Psi}_{\mathrm{s}},\boldsymbol{\Psi}_{\mathrm{a}})=f_{\mathrm{E},i}^{(\mathrm{H})}(\boldsymbol{\Psi}_{\mathrm{s}}+\boldsymbol{\Psi}_{\mathrm{a}})-f_{\mathrm{E},i}^{(\mathrm{H})}(\boldsymbol{\Psi}_{\mathrm{a}}),\tag{29}$$

where $f_{\mathrm{B}}^{(\mathrm{H})}$ and $f_{\mathrm{E},i}^{(\mathrm{H})}$ are defined according to Eqs. (18) and (19) as

$$f_{\mathrm{B}}^{(\mathrm{H})}(\boldsymbol{Y})=\log_2\det\left(\boldsymbol{I}+\boldsymbol{\Lambda}\boldsymbol{Y}\right),\tag{30}$$

$$\begin{aligned}&f_{\mathrm{E},i}^{(\mathrm{H})}(\boldsymbol{Y})\\=&\mathbb{E}\left[\log_2\det\left(\boldsymbol{I}+\boldsymbol{W}_i\boldsymbol{\Sigma}_i^{1/2}\boldsymbol{V}_{\mathrm{H}}\boldsymbol{Y}\boldsymbol{V}_{\mathrm{H}}^{\dagger}\boldsymbol{\Sigma}_i^{1/2}\boldsymbol{W}_i^{\dagger}\right)\right].\end{aligned}\tag{31}$$

Accordingly, when $\tilde{\boldsymbol{V}}=\boldsymbol{V}_{\mathrm{H}}$, the $\{\boldsymbol{\Psi}_{\mathrm{s}},\boldsymbol{\Psi}_{\mathrm{a}}\}$-optimizing sub-problem can be denoted as

$$\max_{\boldsymbol{\Psi}_{\mathrm{s}},\boldsymbol{\Psi}_{\mathrm{a}}\succeq\boldsymbol{0}}[R_{\mathrm{s}}^{(\mathrm{H})}(\boldsymbol{\Psi}_{\mathrm{s}},\boldsymbol{\Psi}_{\mathrm{a}})]^{+}\tag{32a}$$

$$\text{s.t. } 0\le\Psi_{\mathrm{p}}^{[kk]}\le\Gamma_{\mathrm{s}},\ k=1,2,\ldots,K,\tag{32b}$$

$$0\le\mathrm{tr}\left(\boldsymbol{G}\boldsymbol{V}_{\mathrm{H}}(\boldsymbol{\Psi}_{\mathrm{s}}+\boldsymbol{\Psi}_{\mathrm{a}})\boldsymbol{V}_{\mathrm{H}}^{\dagger}\boldsymbol{G}^{\dagger}\right)\le\Gamma_{\mathrm{I}},\tag{32c}$$

where $\boldsymbol{\Psi}_{\mathrm{p}}=\boldsymbol{V}_{\mathrm{H}}(\boldsymbol{\Psi}_{\mathrm{s}}+\boldsymbol{\Psi}_{\mathrm{a}})\boldsymbol{V}_{\mathrm{H}}^{\dagger}$.

Similarly, when $\tilde{\boldsymbol{V}}=\boldsymbol{V}_{\mathrm{G}}$, the secrecy rate can be written as

$$R_{\mathrm{s}}^{(\mathrm{G})}(\boldsymbol{\Psi}_{\mathrm{s}},\boldsymbol{\Psi}_{\mathrm{a}})=R_{\mathrm{B}}^{(\mathrm{G})}(\boldsymbol{\Psi}_{\mathrm{s}},\boldsymbol{\Psi}_{\mathrm{a}})-\max_{1\le i\le L}R_{\mathrm{E},i}^{(\mathrm{G})}(\boldsymbol{\Psi}_{\mathrm{s}},\boldsymbol{\Psi}_{\mathrm{a}}),\tag{33}$$

where the superscript (G) denotes null-space precoding in the eigen-direction of the eavesdropping channel $\boldsymbol{G}$. According to Eqs. (16) and (17), the information rates $R_{\mathrm{B}}^{(\mathrm{G})}$ and $R_{\mathrm{E},i}^{(\mathrm{G})}$ with AN injection are given as

$$R_{\mathrm{B}}^{(\mathrm{G})}(\boldsymbol{\Psi}_{\mathrm{s}},\boldsymbol{\Psi}_{\mathrm{a}})=f_{\mathrm{B}}^{(\mathrm{G})}(\boldsymbol{\Psi}_{\mathrm{s}}+\boldsymbol{\Psi}_{\mathrm{a}})-f_{\mathrm{B}}^{(\mathrm{G})}(\boldsymbol{\Psi}_{\mathrm{a}}),\tag{34}$$

$$R_{\mathrm{E},i}^{(\mathrm{G})}(\boldsymbol{\Psi}_{\mathrm{s}},\boldsymbol{\Psi}_{\mathrm{a}})=f_{\mathrm{E},i}^{(\mathrm{G})}(\boldsymbol{\Psi}_{\mathrm{s}}+\boldsymbol{\Psi}_{\mathrm{a}})-f_{\mathrm{E},i}^{(\mathrm{G})}(\boldsymbol{\Psi}_{\mathrm{a}}),\tag{35}$$

where $f_{\mathrm{B}}^{(\mathrm{G})}$ and $f_{\mathrm{E},i}^{(\mathrm{G})}$ are defined according to Eqs. (18) and (19) as

$$f_{\mathrm{B}}^{(\mathrm{G})}(\boldsymbol{Y})=\log_2\det\left(\boldsymbol{I}+\boldsymbol{V}_{\mathrm{H}}\boldsymbol{\Lambda}\boldsymbol{V}_{\mathrm{H}}^{\dagger}\boldsymbol{V}_{\mathrm{G}}\boldsymbol{Y}\boldsymbol{V}_{\mathrm{G}}^{\dagger}\right),\tag{36}$$

$$\begin{aligned}&f_{\mathrm{E},i}^{(\mathrm{G})}(\boldsymbol{Y})\\=&\mathbb{E}\left[\log_2\det\left(\boldsymbol{I}+\boldsymbol{W}_i\boldsymbol{\Sigma}_i^{1/2}\boldsymbol{V}_{\mathrm{G}}\boldsymbol{Y}\boldsymbol{V}_{\mathrm{G}}^{\dagger}\boldsymbol{\Sigma}_i^{1/2}\boldsymbol{W}_i^{\dagger}\right)\right].\end{aligned}\tag{37}$$

Accordingly, in the case of $\tilde{\boldsymbol{V}}=\boldsymbol{V}_{\mathrm{G}}$, the $\{\boldsymbol{\Psi}_{\mathrm{s}},\boldsymbol{\Psi}_{\mathrm{a}}\}$-optimizing sub-problem can be denoted as

$$\max_{\boldsymbol{\Psi}_{\mathrm{s}},\boldsymbol{\Psi}_{\mathrm{a}}\succeq\boldsymbol{0}}[R_{\mathrm{s}}^{(\mathrm{G})}(\boldsymbol{\Psi}_{\mathrm{s}},\boldsymbol{\Psi}_{\mathrm{a}})]^{+}\tag{38a}$$

$$\text{s.t. } 0\le\Psi_{\mathrm{p}}^{[kk]}\le\Gamma_{\mathrm{s}},\ k=1,2,\ldots,K,\tag{38b}$$

where $\boldsymbol{\Psi}_{\mathrm{p}}=\boldsymbol{V}_{\mathrm{G}}(\boldsymbol{\Psi}_{\mathrm{s}}+\boldsymbol{\Psi}_{\mathrm{a}})\boldsymbol{V}_{\mathrm{G}}^{\dagger}$.

4 Difference convex program and iterative outer approximation method

The secrecy rate maximization problems (32) and (38) are non-convex because both $R_{\mathrm{B}}^{(x)}$ and $R_{\mathrm{E}}^{(x)}$ ($x\in\{\mathrm{H},\mathrm{G}\}$) are the differences of two concave functions. Next, we show that each of the problems can be converted into a CDC program, and solved by the iterative outer approximation method. Specifically, by replacing $R_{\mathrm{E},i}^{(x)}$ with the approximation (21), the optimizing function $R_{\mathrm{s}}^{(x)}(\boldsymbol{\Psi}_{\mathrm{s}},\boldsymbol{\Psi}_{\mathrm{a}})$ in Eq. (32) or (38) can be approximated as

$$\begin{aligned}R_{\mathrm{s}}^{(x)}(\boldsymbol{\Psi}_{\mathrm{s}},\boldsymbol{\Psi}_{\mathrm{a}})\approx&\widetilde{R}_{\mathrm{s}}^{(x)}(\boldsymbol{\Psi}_{\mathrm{s}},\boldsymbol{\Psi}_{\mathrm{a}})\\=&f_{\mathrm{B}}^{(x)}(\boldsymbol{\Psi}_{\mathrm{s}}+\boldsymbol{\Psi}_{\mathrm{a}})-f_{\mathrm{B}}^{(x)}(\boldsymbol{\Psi}_{\mathrm{a}})\\&-\max_{1\le i\le L}\left\{\widetilde{f}_{\mathrm{E},i}(\boldsymbol{\Psi}_{\mathrm{s}}+\boldsymbol{\Psi}_{\mathrm{a}})-\widetilde{f}_{\mathrm{E},i}(\boldsymbol{\Psi}_{\mathrm{a}})\right\}.\end{aligned}\tag{39}$$

Note that due to the observations in Fig. 3, $\widetilde{R}_{\mathrm{s}}^{(x)}$ tends to be the lower bound of $R_{\mathrm{s}}^{(x)}$ and optimizing $\widetilde{R}_{\mathrm{s}}^{(x)}$ yields the lower bound of the maximum secrecy rate in Eqs. (32) and (38).

We rewrite $\widetilde{f}_{\mathrm{E},i}(\boldsymbol{\Psi}_{\mathrm{s}}+\boldsymbol{\Psi}_{\mathrm{a}})$ in Eq. (39) as

$$\widetilde{f}_{\mathrm{E},i}(\boldsymbol{\Psi}_{\mathrm{s}}+\boldsymbol{\Psi}_{\mathrm{a}})=\sum_{j=1}^{L}\widetilde{f}_{\mathrm{E},j}(\boldsymbol{\Psi}_{\mathrm{s}}+\boldsymbol{\Psi}_{\mathrm{a}})-\sum_{j=1,j\ne i}^{L}\widetilde{f}_{\mathrm{E},j}(\boldsymbol{\Psi}_{\mathrm{s}}+\boldsymbol{\Psi}_{\mathrm{a}}).$$

The first term is independent of the index i and can be pulled out of the maximization in Eq. (39), thus becoming

$$\widetilde{R}_{\mathrm{s}}^{(x)}(\boldsymbol{\Psi}_{\mathrm{s}},\boldsymbol{\Psi}_{\mathrm{a}})=-p^{(x)}(\boldsymbol{\Psi}_{\mathrm{s}},\boldsymbol{\Psi}_{\mathrm{a}})+q^{(x)}(\boldsymbol{\Psi}_{\mathrm{s}},\boldsymbol{\Psi}_{\mathrm{a}}),\tag{40}$$

where

$$p^{(x)}(\boldsymbol{\Psi}_{\rm s},\boldsymbol{\Psi}_{\rm a})=\max_{1\le i\le L}\Big\{-f_{\rm B}^{(x)}(\boldsymbol{\Psi}_{\rm s}+\boldsymbol{\Psi}_{\rm a})-\widetilde{f}_{{\rm E},i}(\boldsymbol{\Psi}_{\rm a})-\sum_{j=1,j\neq i}^{L}\widetilde{f}_{{\rm E},j}(\boldsymbol{\Psi}_{\rm s}+\boldsymbol{\Psi}_{\rm a})\Big\},\tag{41}$$

$$q^{(x)}(\boldsymbol{\Psi}_{\rm s},\boldsymbol{\Psi}_{\rm a})=-\sum_{j=1}^{L}\widetilde{f}_{{\rm E},j}(\boldsymbol{\Psi}_{\rm s}+\boldsymbol{\Psi}_{\rm a})-f_{\rm B}^{(x)}(\boldsymbol{\Psi}_{\rm a}).\tag{42}$$

As maximization and summation of a finite number of functions are convex-preserving, both $p^{(x)}(\cdot)$ and $q^{(x)}(\cdot)$ are convex. Next, we introduce the auxiliary variables t and s such that

$$p^{(x)}(\boldsymbol{\Psi}_{\rm s},\boldsymbol{\Psi}_{\rm a})-q^{(x)}(\boldsymbol{\Psi}_{\rm s},\boldsymbol{\Psi}_{\rm a})\le t,\tag{43}$$

$$\Longrightarrow p^{(x)}(\boldsymbol{\Psi}_{\rm s},\boldsymbol{\Psi}_{\rm a})+s-s-t-q^{(x)}(\boldsymbol{\Psi}_{\rm s},\boldsymbol{\Psi}_{\rm a})\le 0,\tag{44}$$

where $t\le 0$ and s is real. Inequality (44) can be rewritten as the following system of inequalities:

$$\begin{cases}s+p^{(x)}(\boldsymbol{\Psi}_{\rm s},\boldsymbol{\Psi}_{\rm a})\le 0,\\ t+s+q^{(x)}(\boldsymbol{\Psi}_{\rm s},\boldsymbol{\Psi}_{\rm a})\ge 0.\end{cases}\tag{45}$$

Comparing inequality (43) with Eq. (40), instead of maximizing $\widetilde{R}_{\rm s}^{(x)}(\boldsymbol{\Psi}_{\rm s},\boldsymbol{\Psi}_{\rm a})$ directly, we can alternatively minimize the auxiliary variable t. Combining the inequality constraints (45) with the power constraint in inequality (32b) and the interference constraint in inequality (32c), while assuming eigenspace precoder $\boldsymbol{V}_{\rm H}$, the secrecy rate maximization (32), with $R_{\rm s}^{({\rm H})}$ replaced by its approximation $\widetilde{R}_{\rm s}^{({\rm H})}$, is equivalent to the CDC program (Horst and Tuy, 1996) given as follows:

$$\begin{aligned}&\min\ t\\ &\text{s.t. } h^{({\rm H})}(\boldsymbol{w})=\max\Big\{s+p^{({\rm H})}(\boldsymbol{\Psi}_{\rm s},\boldsymbol{\Psi}_{\rm a}),\ t,\\ &\Psi_{\rm p}^{[kk]}-\Gamma_{\rm s},\ {\rm tr}\left(\boldsymbol{G}\boldsymbol{V}_{\rm H}(\boldsymbol{\Psi}_{\rm s}+\boldsymbol{\Psi}_{\rm a})\boldsymbol{V}_{\rm H}^{\dagger}\boldsymbol{G}^{\dagger}\right)-\Gamma_{\rm I}\Big\},\\ &\qquad k=1,2,\ldots,K,\\ &g^{({\rm H})}(\boldsymbol{w})=t+s+q^{({\rm H})}(\boldsymbol{\Psi}_{\rm s},\boldsymbol{\Psi}_{\rm a})\ge 0.\end{aligned}\tag{46}$$

On the other hand, using the null-space precoder $\boldsymbol{V}_{\rm G}$, the secrecy rate optimization problem becomes

$$\begin{aligned}&\min\ t\\ &\text{s.t. } h^{({\rm G})}(\boldsymbol{w})=\max\Big\{s+p^{({\rm G})}(\boldsymbol{\Psi}_{\rm s},\boldsymbol{\Psi}_{\rm a}),\ t,\\ &\Psi_{\rm p}^{[kk]}-\Gamma_{\rm s}\Big\},\ k=1,2,\ldots,K,\\ &g^{({\rm G})}(\boldsymbol{w})=t+s+q^{({\rm G})}(\boldsymbol{\Psi}_{\rm s},\boldsymbol{\Psi}_{\rm a})\ge 0,\end{aligned}\tag{47}$$

where the tuple $\boldsymbol{w}=\{\boldsymbol{\Psi}_{\rm a},\boldsymbol{\Psi}_{\rm s},s,t\}$ and we denote $t_{\boldsymbol{w}}\equiv t$.

Both problems (46) and (47) can be solved by the iterative outer approximation method (Horst and Tuy, 1996), as collectively outlined in Algorithm 1. For notational convenience, we denote the sets $H^{(x)}=\{\boldsymbol{w}:h^{(x)}(\boldsymbol{w})\le 0\}$, $G^{(x)}=\{\boldsymbol{w}:g^{(x)}(\boldsymbol{w})\ge 0\}$, and $\partial G^{(x)}=\{\boldsymbol{w}:g^{(x)}(\boldsymbol{w})=0\}$ as the boundary of $G^{(x)}$. The boundary $\partial G^{(x)}$ can be determined by linear interpolation between an inner point $\boldsymbol{x}$ ($\boldsymbol{x}\in G^{(x)}$) and an outer point $\boldsymbol{v}$ ($\boldsymbol{v}\notin G^{(x)}$), where $g^{(x)}(\boldsymbol{x})>0$, $g^{(x)}(\boldsymbol{v})<0$, and $t_{\boldsymbol{v}}<\min\{t_{\boldsymbol{w}}:\boldsymbol{w}\in H^{(x)}\cap G^{(x)}\}$. An example of such an outer point $\boldsymbol{v}$ can be found by setting $\boldsymbol{\Psi}_{\rm s}=\boldsymbol{\Psi}_{\rm wf}$, $\boldsymbol{\Psi}_{\rm a}=\boldsymbol{0}$, and

$$\boldsymbol{v}=\Big\{\boldsymbol{0},\boldsymbol{\Psi}_{\rm wf},\min_{1\le i\le L}\sum_{j=1,j\neq i}^{L}\widetilde{R}_{{\rm E},j}(\boldsymbol{\Psi}_{\rm wf},\boldsymbol{0})-R_{\rm B}^{(x)}(\boldsymbol{\Psi}_{\rm wf},\boldsymbol{0})\Big\}.$$

Denote $\pi(\boldsymbol{x})=v\boldsymbol{x}+(1-v)\boldsymbol{v}$ $(0<v<1)$ as the intersection point between the line segment $[\boldsymbol{x},\boldsymbol{v}]$ and the boundary $\partial G^{(x)}$, i.e., $g^{(x)}(\pi(\boldsymbol{x}))=0$. Because $g^{(x)}(\cdot)$ is convex, $\pi(\boldsymbol{x})$ can be uniquely obtained by an univariate convex minimization $\min\{v:\pi(\boldsymbol{x})\in G^{(x)}\}$. In the initialization of Algorithm 1, the inner point $\boldsymbol{w}_0$ can be determined by running an algorithm to solve the convex maximization problem $\max\{g^{(x)}(\boldsymbol{x}):\boldsymbol{x}\in H^{(x)}\}$ until a feasible point $\boldsymbol{x}_0$ is found, if it exists. We then set the initial state $\boldsymbol{w}_0=\pi(\boldsymbol{x}_0)$.

Because the monomial $t\le 0$ and $g^{(x)}(\boldsymbol{w})\ge 0$ (Horst and Tuy, 1996, Lemma X.2), the CDC problems (46) and (47) are stable in the sense of Def. X.1 in Horst and Tuy (1996). Therefore, the convergence of Algorithm 1 can be easily guaranteed (Horst and Tuy, 1996, Prop. X.3). Note that Algorithm 1 may require infinite iterations to converge to the global optimal solution. Therefore, a relaxation parameter $\epsilon\ge 0$ is introduced (line 5), which provides a trade-off between optimality and complexity. Specifically, $\epsilon=0$ corresponds to the global optimal solution of problem (46) or (47).

In addition, we present the computational complexity analysis of the presented iterative outer approximation method. The complexity is composed of two parts, i.e., the complexity of solving the subproblem (line 4) and the complexity of acquiring the

Algorithm 1 Optimal power allocation

1: **Initialization**
2: Determine a feasible solution $\boldsymbol{w}_0 \in H^{(x)} \cap \partial G^{(x)}$
3: **for** $k \geq 1$ **do**
4: Solve the sub-problem

$$\boldsymbol{z}_k = \arg\max_{\boldsymbol{z}} \{g^{(x)}(\boldsymbol{z}) : h^{(x)}(\boldsymbol{z}) \leq 0, t_{\boldsymbol{z}} \leq t_{\boldsymbol{w}_{k-1}}\}$$

5: **if** $g^{(x)}(\boldsymbol{z}_k) \geq \epsilon$ **then**
6: $\boldsymbol{w}_k = \pi(\boldsymbol{z}_k)$, $k \to k+1$
7: **else**
8: Set the output $\boldsymbol{w}^* = \boldsymbol{z}_k$
9: **return**
10: **end if**
11: **end for**

optimal interpolation factor v (line 6). Because the sub-problem (line 4) has been verified to be convex, it is solved using the inner point method (IPM) in the CVX toolbox. According to the arithmetic complexity of the linear programming by IPM shown in Ben-Tal and Nemirovski (2001), the complexity of the power allocation sub-problem (line 4) is scaled as $\mathcal{O}\left((3K+6)^{3/2}(2K+2)^2\right)$, where K is the number of transmitting nodes of Alice. Similarly, the complexity of solving the optimal interpolation sub-problem (line 6) is $\mathcal{O}\left((m+n)^{3/2}n^2\right)$ with $n=1$ and $m=1$, which can be neglected. We denote T as the number of iterations of Algorithm 1 under the relaxation parameter ϵ. Therefore, while retaining only the highest-order term, the overall complexity of solving this CDC problem can be scaled as $\mathcal{O}\left(TK^{3.5}\right)$.

5 Underlaid secure precoding for the large-dimensional C-MIMO system

As we all know, the large number of connections is one of the crucial characteristics of IIoT. However, the complexity of the proposed EAP method exponentially increases with the increase of the transmit nodes, which is not adaptive to the large-dimensional scenario. Therefore, we further consider designing a simplified version of the EAP method for the large-dimensional underlaid C-MIMO system by adopting uniform power allocation, where the precoder is selected from the two sets of eigenvectors:

1. Null-space AN injection precoding $\boldsymbol{V}_{\mathrm{H}}^{\mathrm{null}}$

When $K >> N$, the null-space of the main channel exists, and can be used to precode the AN and eliminate the interference of AN at the legitimate receiver (Goel and Negi, 2008; Zhou and McKay, 2010; Zhang et al., 2013; Zhu Y et al., 2013; Zheng TX et al., 2015). Let $\boldsymbol{V}_{\mathrm{s}} = \boldsymbol{V}_{\mathrm{H}}[:, 1:N] \in \mathbb{C}^{K\times N}$ and $\boldsymbol{V}_{\mathrm{a}} = \boldsymbol{V}_{\mathrm{H}}^{\mathrm{null}} = \boldsymbol{V}_{\mathrm{H}}[:, N+1:K] \in \mathbb{C}^{K\times(K-N)}$, where the columns of $\boldsymbol{V}_{\mathrm{H}}$ are the right singular vectors of the main channel $\boldsymbol{H}$, i.e., $\boldsymbol{H} = \boldsymbol{U}_{\mathrm{H}}\boldsymbol{\Lambda}_{\mathrm{H}}^{1/2}\boldsymbol{V}_{\mathrm{H}}^{\dagger}$. Additionally, the uniform power allocation is used, i.e., $\Psi_{\mathrm{s}}^{[kk]} = \psi_{\mathrm{s}}$ $(k = 1, 2, \ldots, N)$ and $\Psi_{\mathrm{a}}^{[kk]} = \psi_{\mathrm{a}}$ $(k = N+1, N+2, \ldots, K)$. Herein, only the scalars ψ_{s} and ψ_{a} should be optimized to maximize the secrecy rate of this CR system.

2. Orthogonal subspace projection precoding $\boldsymbol{V}_{\mathrm{G}}^{\mathrm{eff}}$

To avoid interference toward the PU, the signals and AN can be precoded in the null-space of the interference channel $\boldsymbol{G}$. When $K >> N$, the $\boldsymbol{V}_{\mathrm{G}}$ method, which selects the null-subspaces for constructing the precoder would result in relatively poor performance, because the choice of basis may potentially be orthogonal to the signals. Therefore, this issue can be solved by selecting a set of basis vectors in the null-space of $\boldsymbol{G}$ that tend to align with the eigenspace of the main channel (Rajashekar and Hanzo, 2017). Specifically, let $\boldsymbol{V}_{\mathrm{G}}^{\mathrm{null}} = \boldsymbol{V}_{\mathrm{G}}[:, l+1:K]$ and $\boldsymbol{V}_{\mathrm{H}}^{\mathrm{sub}} = \boldsymbol{V}_{\mathrm{H}}[:, 1:l], l = 1, 2, \ldots, K$, where l denotes the number of sub-channels chosen to transmit the signals and AN. Note that $\boldsymbol{V}_{\mathrm{G}}^{\mathrm{null}}$ corresponds to the orthogonal column space of $\boldsymbol{G}$ and $\boldsymbol{V}_{\mathrm{H}}^{\mathrm{sub}}$ corresponds to the column space of $\boldsymbol{H}$. Let $\boldsymbol{P}_{\mathrm{G}}^{\mathrm{null}} = \boldsymbol{V}_{\mathrm{G}}^{\mathrm{null}}(\boldsymbol{V}_{\mathrm{G}}^{\mathrm{null}})^{\dagger}$ and $\boldsymbol{P}_{\mathrm{H}}^{\mathrm{sub}} = (\boldsymbol{V}_{\mathrm{H}}^{\mathrm{sub}})^{\dagger}$ denote the projection matrices associated with $\boldsymbol{V}_{\mathrm{G}}^{\mathrm{null}}$ and $\boldsymbol{V}_{\mathrm{H}}^{\mathrm{sub}}$, respectively. Considering $\overline{\boldsymbol{P}} = \boldsymbol{P}_{\mathrm{H}}^{\mathrm{sub}}\boldsymbol{P}_{\mathrm{G}}^{\mathrm{null}} = \overline{\boldsymbol{U}}\overline{\boldsymbol{\Lambda}}^{1/2}\overline{\boldsymbol{V}}^{\dagger}$, the subspace projection precoder $\boldsymbol{V}_{\mathrm{G}}^{\mathrm{eff}}$ can be written as

$$\boldsymbol{V}_{\mathrm{G}}^{\mathrm{eff}} = \overline{\boldsymbol{V}}[:, 1:l] \in \mathbb{C}^{K\times l}.$$

$\boldsymbol{V}_{\mathrm{G}}^{\mathrm{eff}}$ corresponds to the right singular vectors of $\overline{\boldsymbol{P}}$, which can also be acquired by the eigenvalue decomposition as

$$\overline{\boldsymbol{P}}^{\dagger}\overline{\boldsymbol{P}} = \boldsymbol{V}_{\mathrm{G}}^{\mathrm{null}}\boldsymbol{Q}(\boldsymbol{V}_{\mathrm{G}}^{\mathrm{null}})^{\dagger} \in \mathbb{C}^{K\times K},$$

where

$$\boldsymbol{Q} = (\boldsymbol{V}_{\mathrm{G}}^{\mathrm{null}})^{\dagger}\boldsymbol{V}_{\mathrm{H}}^{\mathrm{sub}}(\boldsymbol{V}_{\mathrm{H}}^{\mathrm{sub}})^{\dagger}\boldsymbol{V}_{\mathrm{G}}^{\mathrm{null}} \in \mathbb{C}^{l\times l}.$$

Therefore, let $\boldsymbol{V}_{\mathrm{s}} = \boldsymbol{V}_{\mathrm{G}}^{\mathrm{eff}}[:, 1:r] \in \mathbb{C}^{K\times r}$ $(r = 1, 2, \ldots, l)$ and $\boldsymbol{V}_{\mathrm{a}} = \boldsymbol{V}_{\mathrm{G}}^{\mathrm{eff}}[:, r+1:l] \in \mathbb{C}^{K\times(l-r)}$ $(r = 1, 2, \ldots, l)$ denote the subspace projection precoders for the signals and AN, respectively. Additionally,

because the signals and AN are precoded in the span of $\boldsymbol{V}_{\mathrm{G}}^{\mathrm{null}}$, interference towards the PU is completely eliminated and the maximum transmit powers are set for both the signals and AN, i.e., $\Psi_{\mathrm{s}}^{[kk]}=\psi_{\mathrm{s}}$ $(k=1,2,\dots,r)$ and $\Psi_{\mathrm{a}}^{[kk]}=\psi_{\mathrm{a}}$ $(k=r+1,r+2,\dots,l)$. Herein, the finite discrete variables l, r, and the variables ψ_{s}, ψ_{a} should be optimized to maximize the secrecy rate of this CR system.

According to the $\boldsymbol{V}_{\mathrm{H}}^{\mathrm{null}}$ precoding method, the secrecy rate formulation can be rewritten as

$$\begin{aligned}&R_{\mathrm{s}}^{(\boldsymbol{V}_{\mathrm{H}}^{\mathrm{null}})}(\psi_{\mathrm{s}},\psi_{\mathrm{a}})\\=&R_{\mathrm{B}}^{(\boldsymbol{V}_{\mathrm{H}}^{\mathrm{null}})}(\psi_{\mathrm{s}},\psi_{\mathrm{a}})-\max_{1\le i\le L}R_{\mathrm{E},i}^{(\boldsymbol{V}_{\mathrm{H}}^{\mathrm{null}})}(\psi_{\mathrm{s}},\psi_{\mathrm{a}}),\end{aligned}\tag{48}$$

where

$$\begin{aligned}&R_{\mathrm{B}}^{(\boldsymbol{V}_{\mathrm{H}}^{\mathrm{null}})}(\psi_{\mathrm{s}},\psi_{\mathrm{a}})\\=&\log_2\det\left(\boldsymbol{I}+\boldsymbol{V}_{\mathrm{H}}\boldsymbol{\Lambda}_{\mathrm{H}}\boldsymbol{V}_{\mathrm{H}}^{\dagger}\boldsymbol{V}_{\mathrm{s}}\boldsymbol{\Psi}_{\mathrm{s}}\boldsymbol{V}_{\mathrm{s}}^{\dagger}\right),\end{aligned}\tag{49}$$

$$\begin{aligned}&R_{\mathrm{E},i}^{(\boldsymbol{V}_{\mathrm{H}}^{\mathrm{null}})}(\psi_{\mathrm{s}},\psi_{\mathrm{a}})\\=&\log_2\det\left(\boldsymbol{I}+\boldsymbol{W}_i\boldsymbol{\Sigma}_i^{1/2}(\boldsymbol{V}_{\mathrm{s}}\boldsymbol{\Psi}_{\mathrm{s}}\boldsymbol{V}_{\mathrm{s}}^{\dagger}+\boldsymbol{V}_{\mathrm{a}}\boldsymbol{\Psi}_{\mathrm{a}}\boldsymbol{V}_{\mathrm{a}}^{\dagger})\boldsymbol{\Sigma}_i^{1/2}\boldsymbol{W}_i^{\dagger}\right)\\&-\log_2\det\left(\boldsymbol{I}+\boldsymbol{W}_i\boldsymbol{\Sigma}_i^{1/2}\boldsymbol{V}_{\mathrm{a}}\boldsymbol{\Psi}_{\mathrm{a}}\boldsymbol{V}_{\mathrm{a}}^{\dagger}\boldsymbol{\Sigma}_i^{1/2}\boldsymbol{W}_i^{\dagger}\right).\end{aligned}\tag{50}$$

Therefore, optimization problem (32) can be reformulated as

$$\max_{\psi_{\mathrm{s}}\ge0,\psi_{\mathrm{a}}\ge0}[R_{\mathrm{s}}^{(\boldsymbol{V}_{\mathrm{H}}^{\mathrm{null}})}(\psi_{\mathrm{s}},\psi_{\mathrm{a}})]^{+}\tag{51a}$$

$$\text{s.t. }\Psi_{\mathrm{s}}^{[kk]}=\psi_{\mathrm{s}},k=1,2,\dots,N,\tag{51b}$$

$$\Psi_{\mathrm{a}}^{[kk]}=\psi_{\mathrm{a}},k=N+1,N+2,\dots,K,\tag{51c}$$

$$0\le\Psi_{\mathrm{p}}^{[kk]}\le\Gamma_{\mathrm{s}},k=1,2,\dots,K,\tag{51d}$$

$$0\le\mathrm{tr}\left(\boldsymbol{G}(\boldsymbol{V}_{\mathrm{s}}\boldsymbol{\Psi}_{\mathrm{s}}\boldsymbol{V}_{\mathrm{s}}^{\dagger}+\boldsymbol{V}_{\mathrm{a}}\boldsymbol{\Psi}_{\mathrm{a}}\boldsymbol{V}_{\mathrm{a}}^{\dagger})\boldsymbol{G}^{\dagger}\right)\le\Gamma_{\mathrm{I}},\tag{51e}$$

where $\boldsymbol{\Psi}_{\mathrm{p}}=\boldsymbol{V}_{\mathrm{s}}\boldsymbol{\Psi}_{\mathrm{s}}\boldsymbol{V}_{\mathrm{s}}^{\dagger}+\boldsymbol{V}_{\mathrm{a}}\boldsymbol{\Psi}_{\mathrm{a}}\boldsymbol{V}_{\mathrm{a}}^{\dagger}$.

According to the $\boldsymbol{V}_{\mathrm{G}}^{\mathrm{eff}}$ precoding method, the secrecy rate formulation can be rewritten as

$$\begin{aligned}&R_{\mathrm{s}}^{(\boldsymbol{V}_{\mathrm{G}}^{\mathrm{eff}})}(l,r,\psi_{\mathrm{s}},\psi_{\mathrm{a}})\\=&R_{\mathrm{B}}^{(\boldsymbol{V}_{\mathrm{G}}^{\mathrm{eff}})}(l,r,\psi_{\mathrm{s}},\psi_{\mathrm{a}})-\max_{1\le i\le L}R_{\mathrm{E},i}^{(\boldsymbol{V}_{\mathrm{G}}^{\mathrm{eff}})}(l,r,\psi_{\mathrm{s}},\psi_{\mathrm{a}}),\end{aligned}\tag{52}$$

where

$$\begin{aligned}&R_{\mathrm{B}}^{(\boldsymbol{V}_{\mathrm{G}}^{\mathrm{eff}})}(l,r,\psi_{\mathrm{s}},\psi_{\mathrm{a}})\\=&\log_2\det\left(\boldsymbol{I}+\boldsymbol{V}_{\mathrm{H}}\boldsymbol{\Lambda}_{\mathrm{H}}\boldsymbol{V}_{\mathrm{H}}^{\dagger}(\boldsymbol{V}_{\mathrm{s}}\boldsymbol{\Psi}_{\mathrm{s}}\boldsymbol{V}_{\mathrm{s}}^{\dagger}+\boldsymbol{V}_{\mathrm{a}}\boldsymbol{\Psi}_{\mathrm{a}}\boldsymbol{V}_{\mathrm{a}}^{\dagger})\right)\\&-\log_2\det\left(\boldsymbol{I}+\boldsymbol{V}_{\mathrm{H}}\boldsymbol{\Lambda}_{\mathrm{H}}\boldsymbol{V}_{\mathrm{H}}^{\dagger}\boldsymbol{V}_{\mathrm{a}}\boldsymbol{\Psi}_{\mathrm{a}}\boldsymbol{V}_{\mathrm{a}}^{\dagger}\right),\end{aligned}\tag{53}$$

$$\begin{aligned}&R_{\mathrm{E},i}^{(\boldsymbol{V}_{\mathrm{G}}^{\mathrm{eff}})}(l,r,\psi_{\mathrm{s}},\psi_{\mathrm{a}})\\=&\log_2\det\left(\boldsymbol{I}+\boldsymbol{W}_i\boldsymbol{\Sigma}_i^{1/2}(\boldsymbol{V}_{\mathrm{s}}\boldsymbol{\Psi}_{\mathrm{s}}\boldsymbol{V}_{\mathrm{s}}^{\dagger}+\boldsymbol{V}_{\mathrm{a}}\boldsymbol{\Psi}_{\mathrm{a}}\boldsymbol{V}_{\mathrm{a}}^{\dagger})\boldsymbol{\Sigma}_i^{1/2}\boldsymbol{W}_i^{\dagger}\right)\\&-\log_2\det\left(\boldsymbol{I}+\boldsymbol{W}_i\boldsymbol{\Sigma}_i^{1/2}\boldsymbol{V}_{\mathrm{a}}\boldsymbol{\Psi}_{\mathrm{a}}\boldsymbol{V}_{\mathrm{a}}^{\dagger}\boldsymbol{\Sigma}_i^{1/2}\boldsymbol{W}_i^{\dagger}\right).\end{aligned}\tag{54}$$

Therefore, optimization problem (38) can be reformulated as

$$\max_{l=1,2,\dots,K;r=1,2,\dots,l;\psi_{\mathrm{s}}\ge0;\psi_{\mathrm{a}}\ge0}[R_{\mathrm{s}}^{(\boldsymbol{V}_{\mathrm{G}}^{\mathrm{eff}})}(l,r,\psi_{\mathrm{s}},\psi_{\mathrm{a}})]^{+}\tag{55a}$$

$$\text{s.t. }\Psi_{\mathrm{s}}^{[kk]}=\psi_{\mathrm{s}},\ k=1,2,\dots,r,\tag{55b}$$

$$\Psi_{\mathrm{a}}^{[kk]}=\psi_{\mathrm{a}},\ k=r+1,r+2,\dots,l,\tag{55c}$$

$$0\le\Psi_{\mathrm{p}}^{[kk]}\le\Gamma_{\mathrm{s}},k=1,2,\dots,K,\tag{55d}$$

where $\boldsymbol{\Psi}_{\mathrm{p}}=\boldsymbol{V}_{\mathrm{s}}\boldsymbol{\Psi}_{\mathrm{s}}\boldsymbol{V}_{\mathrm{s}}^{\dagger}+\boldsymbol{V}_{\mathrm{a}}\boldsymbol{\Psi}_{\mathrm{a}}\boldsymbol{V}_{\mathrm{a}}^{\dagger}$.

Although we have simplified optimization problems (32) and (38) by adopting the fixed precoding and uniform power allocation method, it is observed that optimization problems (51) and (55) are still non-convex stochastic ones, for which it is difficult to determine an optimal analytical solution. Instead, we adopt an iterative power allocation algorithm from Lin et al. (2013), which achieves almost the same performance as brute-force search with much lower complexity.

6 Numerical results

In this section, we study the achievable average secrecy rate of the C-MIMO system under both the single antenna power constraint and the interference power constraint toward the PU. A guaranteed minimum distance e_0 is introduced between Alice's head node and any possible location of Eve. To simplify this system, let all the possible locations of Eve be evenly placed on a circle with radius e_0 centered at the transmit head node; i.e., in Eq. (7) we set $e_{1,1}=e_{1,2}=\cdots=e_{L,1}=e_0$. We first simulate the EAP method in a scenario where the legitimate channel does not have the null-space (case 1), i.e., $K=4$, $N_{\mathrm{B}}=4$, $N_{\mathrm{E}}=2$, and $N_{\mathrm{P}}=2$. Then we assume that the legitimate channel has the orthogonal null-space (case 2), i.e., $K=4$, $N_{\mathrm{B}}=2$, $N_{\mathrm{E}}=2$, and $N_{\mathrm{P}}=2$. In cases 1 and 2, the single antenna power constraint is Γ_{s}=23 dBm. Additionally, the performance of the low-powered and large-dimensional C-MIMO system is evaluated (case 3), i.e., $K=64$, $N_{\mathrm{B}}=4$, $N_{\mathrm{E}}=2$, and $N_{\mathrm{P}}=2$. In case 3, the single antenna power constraint is Γ_{s}=13 dBm.

Fig. 4 shows the average secrecy rate of the C-MIMO system achieved by the $\boldsymbol{V}_{\mathrm{H}}$, $\boldsymbol{V}_{\mathrm{G}}$, and EAP methods with the AN injection in case 1 when e_0=10 m, r=3 m. It is observed that the proposed EAP method outperforms both the $\boldsymbol{V}_{\mathrm{H}}$ and $\boldsymbol{V}_{\mathrm{G}}$ methods. Specifically, when the interference constraint dominates the problem, e.g., Γ_{I}=−25 dBm, the EAP method can improve the secrecy rate by about 0.25 nats/(s·Hz) compared to the $\boldsymbol{V}_{\mathrm{H}}$ method. Meanwhile, when the single antenna power constraint Γ_{s} dominates the problem, e.g., Γ_{s}=23 dBm and Γ_{I}=−15 dBm, the EAP method can improve the secrecy rate by about 1.2 nats/(s·Hz) compared to the $\boldsymbol{V}_{\mathrm{G}}$ method. Therefore, the proposed EAP method can adaptively choose an eigenspace that achieves a better secrecy rate than the $\boldsymbol{V}_{\mathrm{H}}$ and $\boldsymbol{V}_{\mathrm{G}}$ methods.

Fig. 5 shows the cumulative distribution functions (CDFs) of the secrecy rates of the C-MIMO system via the EAP method in case 1 when r=3 m and e_0=10 m. The interference power constraint is Γ_{I}=−25, −20, and −15 dBm. Results show that the EAP method can eliminate the secrecy outage under different interference constraints, and that the gain benefits from the AN injection are limited when the interference power is rigorously constrained. Additionally, the fluctuation caused by random propagation fading increases with the relaxation of the interference power constraint.

Fig. 6 shows the CDFs of the secrecy rates via the EAP method in case 1 when r=3 m, Γ_{I}=−15 dBm, and e_0 = 6, 8, and 10 m. Results show that with the increase of e_0, the secrecy rate increases and the performance gain of AN gradually decreases. Moreover, the EAP method with AN injection can fully eliminate the secrecy outage even when the eavesdroppers are distributed on a circle around the transmit cluster with a radius of e_0=6 m.

Fig. 7 shows the CDFs of the secrecy rates via the EAP method in case 1 when e_0=10 m, Γ_{I}=−15 dBm and r=1, 3, and 5 m. Results indicate that the EAP method can eliminate the secrecy outage even when r=1 m; i.e., the cooperative nodes are densely packed together. To further clarify the effect

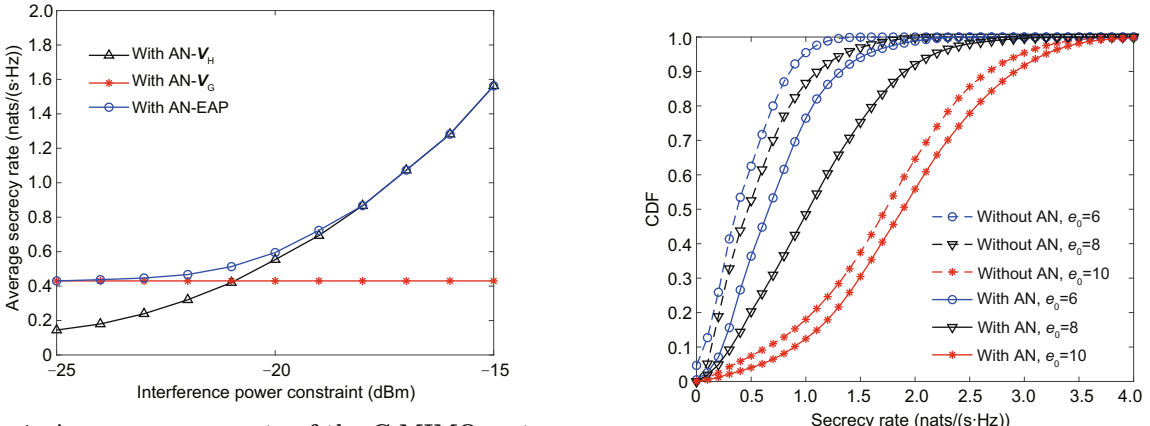

Fig. 4 Average secrecy rate of the C-MIMO system via the $\boldsymbol{V}_{\mathrm{H}}$, $\boldsymbol{V}_{\mathrm{G}}$, and EAP schemes with AN injection under different interference power constraints Γ_{I} when K=4, N_{B}=4, N_{E}=2, N_{P}=2, r=3 m, e_0=10 m, and Γ_{s}=23 dBm (AN: artificial noise; C-MIMO: cooperative multi-input multi-output; EAP: eigenspace-adaptive precoding)

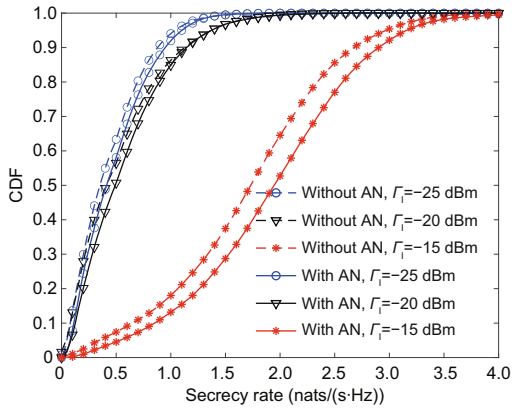

Fig. 5 CDFs of the C-MIMO system secrecy rate via EAP when K=4, N_{B}=4, N_{E}=2, N_{P}=2, r=3 m, e_0=10 m, and Γ_{s}=23 dBm (CDFs: cumulative distribution functions; C-MIMO: cooperative multi-input multi-output; EAP: eigenspace-adaptive precoding)

Fig. 6 CDFs of the C-MIMO system secrecy rate via EAP when K=4, N_{B}=4, N_{E}=2, N_{P}=2, r=3 m, Γ_{s}=23 dBm, and Γ_{I}=−15 dBm (CDFs: cumulative distribution functions; C-MIMO: cooperative multi-input multi-output; EAP: eigenspace-adaptive precoding)

of the distributed node topology and Eve's distribution on the secrecy rate, Fig. 8 shows the average secrecy rates under different configurations of r and e_0, showing that the secrecy rate increases with the increase of the cluster radius r. Furthermore, it is observed that AN injection achieves the maximum gain at r=5 m and e_0=8 m, which demonstrates that AN injection can achieve better secrecy gain when the eavesdropper is closer to the distributed nodes.

Fig. 9 shows the average secrecy rates via the $\boldsymbol{V}_{\mathrm{H}}$, $\boldsymbol{V}_{\mathrm{G}}$, EAP, and generalized AN-aided precoding (Lin et al., 2013) methods in case 2. In Lin et al. (2013), assuming that the perfect CSI of the legitimate channel and only the statistics of the eavesdropper's channel are known at the transmitter, the optimal structure of the precoding is derived. Therein, the power of AN is divided into two parts; one is injected into the same eigenspace as the signal and the other is uniformly injected into the null-space of the legitimate channel $\boldsymbol{H}$. Results show that the proposed EAP method outperforms the other methods when the interference power constraint dominates the problem and achieves almost the same performance as the optimally structured AN-aided precoding method (Lin et al., 2013) when the single antenna power constraint dominates the problem.

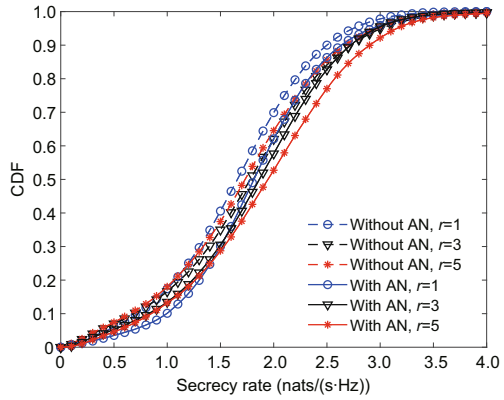

Fig. 7 CDFs of the C-MIMO system secrecy rate via EAP when K=4, N_{B}=4, N_{E}=2, N_{P}=2, e_0=10 m, Γ_{s}=23 dBm, and Γ_{I}=−15 dBm (CDFs: cumulative distribution functions; C-MIMO: cooperative multi-input multi-output; EAP: eigenspace-adaptive precoding)

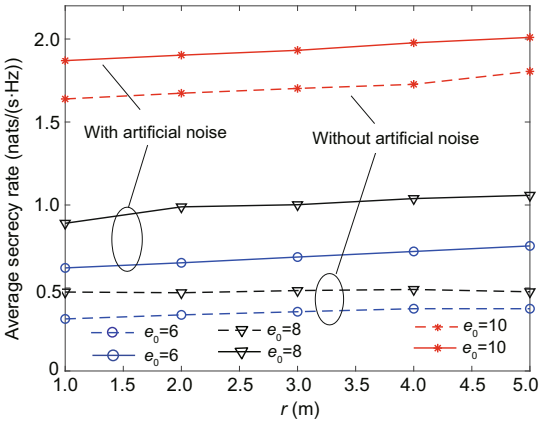

Fig. 8 Average secrecy rate of the C-MIMO system via EAP under different distributed radius r and different eavesdropper-free region e_0, when K=4, N_{B}=4, N_{E}=2, N_{P}=2, Γ_{s}=23 dBm, and Γ_{I}=−15 dBm (C-MIMO: cooperative multi-input multi-output; EAP: eigenspace-adaptive precoding)

Fig. 10 shows the average secrecy rates via the $\boldsymbol{V}_{\mathrm{H}}^{\mathrm{null}}$, $\boldsymbol{V}_{\mathrm{G}}^{\mathrm{eff}}$, and EAP methods in case 3, i.e., the low-powered and large-dimensional C-MIMO system. Therein, the single antenna power constraint is set to Γ_{s}=13 dBm and the interference constraint Γ_{I} is set from −15 to −5 dBm. Results indicate that the large-dimensional C-MIMO can significantly increase the secrecy rate in this underlaid CR system. Similarly, the proposed simplified EAP method for the large-dimensional C-MIMO system can adapt to the more superior eigenspace and achieve a better secrecy rate than both the $\boldsymbol{V}_{\mathrm{H}}^{\mathrm{null}}$ and $\boldsymbol{V}_{\mathrm{G}}^{\mathrm{eff}}$ methods.

7 Conclusions

EAP together with AN-assisted secrecy transmission is considered for a C-MIMO system coexisting with a PU. The design of underlaid secrecy

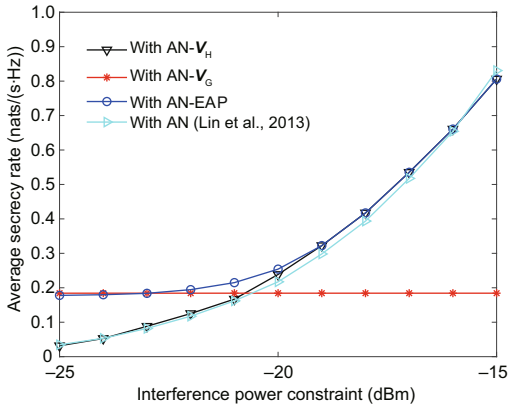

Fig. 9 Average secrecy rate of C-MIMO system via different AN-aided precoding methods when K=4, N_{B}=2, N_{E}=2, N_{P}=2, r=3 m, e_0=10 m, Γ_{s}=23 dBm, and Γ_{I}=−15 dBm (AN: artificial noise; C-MIMO: cooperative multi-input multi-output)

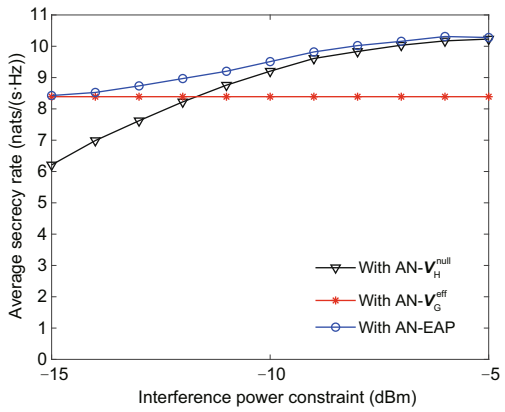

Fig. 10 Average secrecy rate of the large-dimensional C-MIMO system via $\boldsymbol{V}_{\mathbf{H}}^{\mathbf{null}}$, $\boldsymbol{V}_{\mathbf{G}}^{\mathbf{eff}}$, and the simplified EAP methods when K=64, N_B=4, N_E=2, N_P=2, r=3 m, e_0=10 m, and Γ_s=13 dBm (C-MIMO: cooperative multi-input multi-output; EAP: eigenspace-adaptive precoding)

communications exploits the geographical location constraint of the eavesdropper as well as the eigenspace of the channels. Specifically, the eigenvectors are adaptively selected by the transmitter according to the channel conditions. Also, a simplified EAP method is proposed for the large-dimensional C-MIMO system. Numerical results show that the proposed EAP method outperforms the fixed eigenvector precoding method. Moreover, EAP can eliminate the secrecy outage even when the eavesdroppers are located closer to the transmitter. In addition, the simplified EAP method for large-dimensional C-MIMO transmission can significantly improve the secrecy rate with low complexity.

Contributors

Xinyao WANG and Zhong ZHENG designed the research. Xuyan BAO and Yuzhen HUANG processed the data. Xinyao WANG and Zhong ZHENG drafted the paper. Zesong FEI helped organize the paper. Xuyan BAO, Yuzhen HUANG, and Zesong FEI revised and finalized the paper.

Compliance with ethics guidelines

Xinyao WANG, Xuyan BAO, Yuzhen HUANG, Zhong ZHENG, and Zesong FEI declare that they have no conflict of interest.

Data availability

The data that support the findings of this study are available from the corresponding author upon reasonable request.

References

Akhyar F, Lin CY, Muchtar K, et al., 2019. High efficient single-stage steel surface defect detection. Proc 16th IEEE Int Conf on Advanced Video and Signal Based Surveillance, p.1-4. https://doi.org/10.1109/AVSS.2019.8909834

Ben-Tal A, Nemirovski A, 2001. Lectures on Modern Convex Optimization: Analysis, Algorithms, and Engineering Applications. Springer, Philadelphia, USA.

Bloch MR, Laneman JN, 2013. Strong secrecy from channel resolvability. *IEEE Trans Inform Theory*, 59(12):8077-8098. https://doi.org/10.1109/TIT.2013.2283722

Borges PVK, Izquierdo E, 2010. A probabilistic approach for vision-based fire detection in videos. *IEEE Trans Circ Syst Video Technol*, 20(5):721-731. https://doi.org/10.1109/TCSVT.2010.2045813

Chen LW, Chen CR, Chen DE, 2017. VIPS: a video-based indoor positioning system with centimeter-grade accuracy for the IoT. Proc IEEE Int Conf on Pervasive Computing and Communications Workshops, p.63-65. https://doi.org/10.1109/PERCOMW.2017.7917523

Chettri L, Bera R, 2020. A comprehensive survey on Internet of Things (IoT) toward 5G wireless systems. *IEEE Int Things J*, 7(1):16-32. https://doi.org/10.1109/JIOT.2019.2948888

Chiurtu N, Rimoldi B, Telatar E, 2001. On the capacity of multi-antenna Gaussian channels. Proc IEEE Int Symp on Information Theory, p.53-57. https://doi.org/10.1109/ISIT.2001.935916

Csiszar I, Körner J, 1978. Broadcast channels with confidential messages. *IEEE Trans Inform Theory*, 24(3):339-348. https://doi.org/10.1109/TIT.1978.1055892

Deng YS, Wang LF, Zaidi SAR, et al., 2016. Artificial-noise aided secure transmission in large scale spectrum sharing networks. *IEEE Trans Commun*, 64(5):2116-2129. https://doi.org/10.1109/TCOMM.2016.2544300

Fang B, Qian ZP, Shao W, et al., 2016. Precoding and artificial noise design for cognitive MIMOME wiretap channels. *IEEE Trans Veh Technol*, 65(8):6753-6758. https://doi.org/10.1109/TVT.2015.2477305

Goel S, Negi R, 2008. Guaranteeing secrecy using artificial noise. *IEEE Trans Wirel Commun*, 7(6):2180-2189. https://doi.org/10.1109/TWC.2008.060848

Hampel G, Li C, Li JY, 2019. 5G ultra-reliable low-latency communications in factory automation leveraging licensed and unlicensed bands. *IEEE Commun Mag*, 57(5):117-123. https://doi.org/10.1109/MCOM.2019.1601220

He X, Yener A, 2014. MIMO wiretap channels with unknown and varying eavesdropper channel states. *IEEE Trans Inform Theory*, 60(11):6844-6869. https://doi.org/10.1109/TIT.2014.2359192

Hořejší P, Novikov K, Šimon M, 2020. A smart factory in a smart city: virtual and augmented reality in a smart assembly line. *IEEE Access*, 8:94330-94340. https://doi.org/10.1109/ACCESS.2020.2994650

Horst R, Tuy H, 1996. Global Optimization (3rd Ed.). Springer, Berlin, Heidelberg, Germany.

Hu TT, Xiong J, Ma DT, et al., 2018. Optimal and robust AN-aided precoding design for cognitive MIMOME wiretap channels. Proc IEEE/CIC Int Conf on Communications in China, p.500-505. https://doi.org/10.1109/ICCChina.2018.8641254

Hussain T, Muhammad K, Del Ser J, et al., 2020. Intelligent embedded vision for summarization of multiview videos in IIoT. *IEEE Trans Ind Inform*, 16(4):2592-2602. https://doi.org/10.1109/TII.2019.2937905

Lin PH, Lai SH, Lin SC, et al., 2013. On secrecy rate of the generalized artificial-noise assisted secure beamforming for wiretap channels. *IEEE J Sel Areas Commun*, 31(9):1728-1740. https://doi.org/10.1109/JSAC.2013.130907

Lu X, Petrov V, Moltchanov D, et al., 2019. 5G-U: conceptualizing integrated utilization of licensed and unlicensed spectrum for future IoT. *IEEE Commun Mag*, 57(7):92-98. https://doi.org/10.1109/MCOM.2019.1800663

Nguyen DC, Ding M, Pathirana PN, et al., 2022. 6G Internet of Things: a comprehensive survey. *IEEE Int Things J*, 9(1):359-383. https://doi.org/10.1109/JIOT.2021.3103320

Ozgur A, Leveque O, Tse D, 2013. Spatial degrees of freedom of large distributed MIMO systems and wireless ad hoc networks. *IEEE J Sel Areas Commun*, 31(2):202-214. https://doi.org/10.1109/JSAC.2013.130209

Pei YY, Liang YC, Zhang L, et al., 2010. Secure communication over MISO cognitive radio channels. *IEEE Trans Wirel Commun*, 9(4):1494-1502. https://doi.org/10.1109/TWC.2010.04.090746

Rajashekar R, Hanzo L, 2017. Iterative matrix decomposition aided block diagonalization for mm-wave multiuser MIMO systems. *IEEE Trans Wirel Commun*, 16(3):1372-1384. https://doi.org/10.1109/TWC.2016.2628357

Sibomana L, Tran H, Zepernick HJ, 2015. On physical layer security for cognitive radio networks with primary user interference. Proc IEEE Military Communications Conf, p.281-286. https://doi.org/10.1109/MILCOM.2015.7357456

Simon SH, Moustakas AL, Marinelli L, 2006. Capacity and character expansions: moment-generating function and other exact results for MIMO correlated channels. *IEEE Trans Inform Theory*, 52(12):5336-5351. https://doi.org/10.1109/TIT.2006.885519

Sternberg S, 1995. Group Theory and Physics. Cambridge University Press, Cambridge, UK.

Wang HM, Wang C, Ng DWK, et al., 2016. Artificial noise assisted secure transmission for distributed antenna systems. *IEEE Trans Signal Process*, 64(15):4050-4064. https://doi.org/10.1109/TSP.2016.2558164

Wyner AD, 1975. The wire-tap channel. *Bell Syst Techn J*, 54(8):1355-1387. https://doi.org/10.1002/j.1538-7305.1975.tb02040.x

Zhang X, Zhou XY, McKay MR, 2013. On the design of artificial-noise-aided secure multi-antenna transmission in slow fading channels. *IEEE Trans Veh Technol*, 62(5):2170-2181. https://doi.org/10.1109/TVT.2013.2238687

Zheng TX, Wang HM, Yuan JH, et al., 2015. Multiantenna transmission with artificial noise against randomly distributed eavesdroppers. *IEEE Trans Commun*, 63(11):4347-4362. https://doi.org/10.1109/TCOMM.2015.2474390

Zheng Z, Haas ZJ, 2017. On the performance of reconfigurable distributed MIMO in mobile networks. *IEEE Trans Commun*, 65(4):1609-1622. https://doi.org/10.1109/TCOMM.2017.2656129

Zheng Z, Haas ZJ, Kieburg M, 2019. Secrecy rate of cooperative MIMO in the presence of a location constrained eavesdropper. *IEEE Trans Commun*, 67(2):1356-1370. https://doi.org/10.1109/TCOMM.2018.2877329

Zhou XY, McKay MR, 2010. Secure transmission with artificial noise over fading channels: achievable rate and optimal power allocation. *IEEE Trans Veh Technol*, 59(8):3831-3842. https://doi.org/10.1109/TVT.2010.2059057

Zhu FC, Yao ML, 2016. Improving physical-layer security for CRNs using SINR-based cooperative beamforming. *IEEE Trans Veh Technol*, 65(3):1835-1841. https://doi.org/10.1109/TVT.2015.2412152

Zhu Y, Zhou YK, Patel S, et al., 2013. Artificial noise generated in MIMO scenario: optimal power design. *IEEE Signal Process Lett*, 20(10):964-967. https://doi.org/10.1109/LSP.2013.2276042